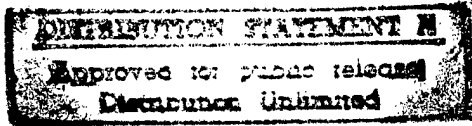


Report No. CG-D-17-96

**PRELIMINARY FIELD TEST RESULTS:
EVALUATION OF INFRARED SENSORS
FOR SURFACE VESSEL
LAW ENFORCEMENT OPERATIONS**

P. SKOWRONEK

U.S. Coast Guard Research and Development Center
1082 Shennecossett Road, Groton, Connecticut 06340-6096



AND

J. V. PLOURDE

Analysis & Technology, Inc.
258 Bank Street, New London, Connecticut 06320



**INTERIM REPORT
DECEMBER 1995**

19961118 179

This document is available to the U.S. public through the
National Technical Information Service, Springfield, Virginia 22161

Prepared for :

**U.S. Department of Transportation
United States Coast Guard
Office of Engineering, Logistics, and Development
Washington, DC 20593-0001**

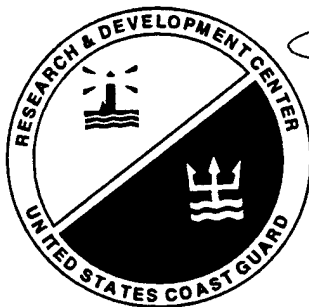
DTIC QUALITY INSPECTED 1


NOTICE

This document is disseminated under the sponsorship of the Department of Transportation in the interest of information exchange. The United States Government assumes no liability for its contents or use thereof.

The United States Government does not endorse products or manufacturers. Trade or manufacturers' names appear herein solely because they are considered essential to the object of this report.

The contents of this report reflect the views of the Coast Guard Research & Development Center. This report does not constitute a standard, specification, or regulation.




G.T. Gunther
Commanding Officer
United States Coast Guard
Research & Development Center
1082 Shennecossett Road
Groton, CT 06340-6096

1. Report No. CG-D-17-96		2. Government Accession No.		3. Recipient's Catalog No.	
4. Title and Subtitle Preliminary Field Test Results: Evaluation Of Infrared Sensors For Surface Vessel Law Enforcements Operations				5. Report Date December 1995	
				6. Performing Organization Code	
				8. Performing Organization Report No. R&DC 06/96	
7. Author(s) P. Skowronek and J.V. Plourde				10. Work Unit No. (TRAIS)	
9. Performing Organization Name and Address USCG R&D Center Analysis & Technology, Inc. 1082 Shennecossett Road 258 Bank Street Groton, CT 06340-6096 New London, CT 06320				11. Contract or Grant No. DTCG39-94-D-E56616	
				13. Type of Report and Period Covered Interim Report June 1995 to Dec 1995	
12. Sponsoring Agency Name and Address Department of Transportation U.S. Coast Guard Office of Engineering, Logistics, and Development Washington, D. C. 20593				14. Sponsoring Agency Code Commandant (G-OLE) USCG Headquarters	
15. Supplementary Notes This report provides documentation of a field test conducted in July 1995 at the Coast Guard Research and Development Center. It is the first of three that will be published in support of the evaluation of Infrared Technology to support the CG Law Enforcement Mission aboard surface vessels.					
16. Abstract <p>During July 1995, the USCG conducted a field evaluation of several commercially available infrared (IR) sensors for their ability to detect low profile surface vessel targets of interest to the law enforcement community. The evaluation was conducted in the target rich area of Long Island Sound between New London, CT and Gardiners Island, NY.</p> <p>The sensors were operated from the roof of the Coast Guard Research and Development Center. Sensors evaluated included the Agema Thermovision 1000 and FLIR Systems SAFIRE operating in the long wave IR (LWIR) and the Aerojet General Thermal Imaging System and Amber Radiance 1 operating in the medium wave IR (MWIR). Each sensor provided a narrow field of view of 2 to 5 degrees, thus permitting comparison of relative performance.</p> <p>Surface truth data were maintained through the use of a GPS tracking system. Environmental conditions were recorded both at the shoreside sensor array and onboard one of the target craft. Radiometric data were recorded for all targets during data collection periods. These data were used to determine the thermal contrast available to the sensors for any target imaging scenario.</p> <p>Analysis of the image data confirmed that all sensors were able to classify targets into general categories at distances up to approximately three nautical miles. While the LWIR sensors were able to detect the targets consistently at distances of 6 to 8 nautical miles, the MWIR sensors outperformed those detection distances by approximately a factor of 2. The relatively high atmospheric moisture content is considered to be the primary cause of these differences.</p>					
17. Key Words Infrared, Infrared Sensors, Infrared Imagers, Long Wave Infrared, Medium Wave Infrared, Low Profile Targets, Law Enforcement, Surface Vessel Law Enforcement			18. Distribution Statement Document is available to the U.S. Public through the National Technical Information Service, Springfield, VA 22161		
19. Security Classif. (of this report) UNCLASSIFIED		20. Security Classif. (of this page) UNCLASSIFIED		21. No. of Pages	
				22. Price	

METRIC CONVERSION FACTORS

Approximate Conversions to Metric Measures

Symbol	When You Know	Multiply By	To Find	Symbol
LENGTH				
in	inches	* 2.5	centimeters	cm
ft	feet	30	centimeters	cm
yd	yards	0.9	meters	m
mi	miles	1.6	kilometers	km
AREA				
in ²	square inches	6.5	square centimeters	cm ²
ft ²	square feet	0.09	square meters	m ²
yd ²	square yards	0.8	square meters	m ²
mi ²	square miles	2.6	square kilometers	km ²
	acres	0.4	hectares	ha
MASS (WEIGHT)				
oz	ounces	28	grams	g
lb	pounds	0.45	kilograms	kg
	short tons (2000 lb)	0.9	tonnes	t
VOLUME				
tsp	teaspoons	5	milliliters	ml
tbsp	tablespoons	15	milliliters	ml
fl oz	fluid ounces	30	milliliters	ml
c	cups	0.24	liters	l
pt	pints	0.47	liters	l
qt	quarts	0.95	liters	l
gal	gallons	3.8	liters	l
ft ³	cubic feet	0.03	cubic meters	m ³
yd ³	cubic yards	0.76	cubic meters	m ³
TEMPERATURE (EXACT)				
°F	Fahrenheit temperature	5/9 (after subtracting 32)	Celsius temperature	°C

* 1 in = 2.54 (exactly).

Approximate Conversions from Metric Measures

Symbol	When You Know	Multiply By	To Find	Symbol
LENGTH				
mm	millimeters	0.4	inches	in
cm	centimeters	0.4	inches	in
m	meters	3.3	feet	ft
m	meters	1.1	yards	yd
km	kilometers	0.6	miles	mi
AREA				
cm ²	square centimeters	0.16	square inches	in ²
m ²	square meters	1.2	square yards	yd ²
km ²	square kilometers	0.4	square miles	mi ²
ha	hectares (10,000 m ²)	2.5	acres	
MASS (WEIGHT)				
g	grams	0.035	ounces	oz
kg	kilograms	2.2	pounds	lb
t	tonnes (1000 kg)	1.1	short tons	
VOLUME				
ml	milliliters	0.03	fluid ounces	fl oz
l	liters	0.125	cups	c
l	liters	2.1	pints	pt
l	liters	1.06	quarts	qt
l	liters	0.26	gallons	gal
m ³	cubic meters	35	cubic feet	ft ³
m ³	cubic meters	1.3	cubic yards	yd ³
TEMPERATURE (EXACT)				
°C	Celsius temperature	9/5 (then add 32)	Fahrenheit temperature	°F

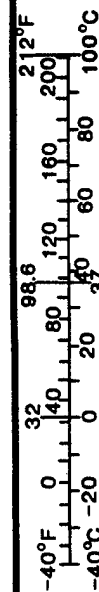


TABLE OF CONTENTS

Section	Page
EXECUTIVE SUMMARY	vii
ACKNOWLEDGMENTS	ix
1.0 INTRODUCTION	1-1
1.1 Purpose	1-1
1.2 Background	1-1
1.3 Field Test Conduct	1-3
1.4 IR Sensor System Descriptions	1-7
1.4.1 LWIR Sensors	1-8
1.4.2 MWIR Sensors	1-9
1.4.3 Video Recording Setup	1-11
1.5 Targets	1-13
1.6 Analysis Procedure	1-13
2.0 DATA ANALYSIS	2-1
2.1 Empirical Detection and Classification Distances	2-1
2.1.1 Empirical Detection Distances	2-1
2.1.2 Empirical Classification Distances	2-2
2.2 Theoretical Detection and Classification Distances	2-3
2.2.1 Theoretical Detection Distances	2-4
2.2.2 Theoretical Classification Distances	2-6
2.3 Correlation of Empirical and Theoretical Distances	2-7
2.3.1 Correlation of Detection Distances	2-7
2.3.2 Correlation of Classification Distances	2-8
3.0 INVESTIGATION OF NON-RESOLUTION RELATED IMAGES	3-1
3.1 Sun Glint	3-1
3.2 Transition Periods	3-3
3.3 Video Polarity	3-7
3.4 Wide Field of View	3-9
3.5 General Image Data and Sensor Performance	3-10
4.0 CONCLUSIONS	4-1
5.0 RECOMMENDATIONS	5-1
REFERENCES	R-1

APPENDICES

Appendix

A OVERVIEW OF IR PHENOMENOLOGY	A-1
--------------------------------------	-----

LIST OF FIGURES

Figure	Page
1-1 Field Test Location	1-5
1-2 Sensor Array Used During July 1995 Field Test	1-7
1-3 IR Data Collection System Schematic	1-12
1-4 Image Data Recorder Workstation	1-12
2-1 Simplified Thermal Scene.....	2-5
2-2 Fundamental Procedure Behind Theoretical Calculations.....	2-5
3-1 MWIR Image of the LICKETY SPLIT Showing Sun Glint.....	3-2
3-2 LWIR Image of the LICKETY SPLIT During Period of MWIR Sun Glint.....	3-2
3-3 Representation of Thermal Transition	3-3
3-4 LWIR Daytime Image of Targets, 19 July 1995	3-5
3-5 MWIR Daytime Image of Targets, 19 July 1995	3-5
3-6 LWIR Nighttime Image of Targets, 24 July 1995	3-6
3-7 MWIR Nighttime Image of Targets, 24 July 1995	3-6
3-8 Black = Hot Video Polarity from All Sensors.....	3-7
3-9 White = Hot Video Polarity from All Sensors.....	3-8
3-10 Demonstration of Wide Field of View from All Sensors.....	3-10
A-1 Radiant Energy versus Wavelength (at 27°C)	A-4
A-2 Atmospheric Transmission versus Wavelength (Range =12 km, RH=50%).....	A-5
A-3 Atmospheric Transmission versus Wavelength (Range =12 km, RH=76%).....	A-5
A-4 Transmitted Power Density versus Wavelength (Range =12 km, RH=50%).....	A-6
A-5 Transmitted Power Density versus Wavelength (Range =12 km, RH=76%).....	A-6

LIST OF TABLES

Table	Page
1-1 Surface Vessel Target Summary	1-6
1-2 Environmental Conditions Experienced.....	1-6
1-3 Summary of Sensor Specifications	1-7
1-4 Amber Radiance 1 Quick-Access Commands	1-11
2-1 Empirical Detection Distances (nmi).....	2-2
2-2 Target Classification Profiles	2-3
2-3 Empirical Classification Distances (nmi).....	2-3
2-4 Theoretical Detection Distances (nmi)	2-6
2-5 Theoretical Classification Distances (nmi)	2-6
2-6 Comparison of Empirical and Theoretical Detection Distances.....	2-8
2-7 Comparison of Empirical and Theoretical Classification Distances.....	2-9

EXECUTIVE SUMMARY

This report documents a United States Coast Guard (USCG) Research and Development (R&D) Center evaluation of an assortment of commercially available infrared (IR) sensor technologies for their utility in supporting detection and classification requirements of the surface vessel law enforcement community. The evaluation was conducted with the sensor array mounted on the top of the USCG R&D Center overlooking the test range established in Long Island Sound. Targets selected for the evaluation consisted of low-profile pleasure craft, a commercial fishing vessel, a sailboat and a rubber liferaft. IR image data were collected during both daytime and nighttime data collection sorties.

Infrared imaging is the technology of viewing a scene by looking at its temperature differences. Observing and analyzing the images allows the operator to discriminate vessel features for classification and detection. The result is a collection of video which appears similar to a television video. To ensure experimental validity, environmental conditions and target and background radiometric data were collected during each IR image data collection period.

A representative cross-sampling of commercially available, cooled IR systems were selected for the test. The systems tested were: FLIR Systems Inc. SAFIRE, Amber Engineering Radiance 1, AGEMA Thermovision 1000, and the Aerojet General Thermal Imager. These systems represented the state of the market for the summer of 1995 and utilize both the mid-wave (MWIR) and long-wave (LWIR) regions of the IR band. The sensors were mounted on the roof of the R&D Center in such a way as to permit collection of IR data images from the same location, simultaneously. This limited the number of variables to be considered during comparison of sensor image data. Data was stored on S-VHS video tape. The experiment was conducted from 17 through 28 July 1995. Six daytime and 3 nighttime data collection periods were conducted.

Generally, conditions were hazy, hot and humid which were a fair simulation of conditions expected during Caribbean operations.

All systems, except the FSI SAFIRE, which had a larger FOV and had a malfunction in the focus travel screw, were capable of classifying the targets between three and five nautical miles on the various days. Detection ranges exhibited greater variance between the systems. LWIR transmission was affected by the atmospheric humidity and the sensors operating at this wavelength were unable to detect any scene detail beyond approximately 5.5 nautical miles while the MWIR sensors were able to consistently detect the targets well beyond this distance.

Several conclusions have been drawn based on the data analyzed to date. In general, MWIR sensors did not experience the signal loss that affected LWIR sensors during the relatively high humid atmospheric conditions experienced during the test. Daytime solar reflections created significant scene clutter for MWIR systems, while having little or no effect on LWIR systems. Comparison of the fields of view (FOV) available demonstrated that a narrow FOV of 2.0 degrees or less for target discrimination and a wide FOV of approximately 7.0 degrees for wide angle searches were preferable. Finally, it is possible to reasonably estimate detection and classification ranges for specific sensors if system characteristics and atmospheric conditions are known.

The main body of this paper includes several printed images demonstrating: the concept of sun glint, thermal transition periods, the similarity of images in reversed polarity, a demonstration of the wide field of view offered by each sensor, and a summary of sensor operator field comments. More complete analysis of these and other features will be included in the final report expected in the summer of 1996. The final report will include a critical review of associated sensor devices that greatly affect the imaging quality of these sensors. The specific devices to be examined are the stabilization systems, auto-trackers, laser rangefinders, and sensor optics.

ACKNOWLEDGMENTS

This evaluation would not have been possible without the contributions of many individuals and organizations. The authors wish to acknowledge the generous support of Dr. Richard Paolino of the Coast Guard Academy and Mr. Gary Hover of the R&D Center who lent their experience and understanding of IR physics through all phases of the evaluation. Their skill, patience and educated perspectives are very much appreciated. Special thanks to Ens. Carlton Williams of the R&D Center and Mr. Jeff Howe, Mr. Chris Oates, Mr. Steve Ricard, and Mr. Gary Reas of Analysis & Technology, Inc. for their assistance during the data collection phase of this project.

For providing the IR sensors used during the data collection, the assistance of Mr. Robert Schellhase of Aerojet General, Inc.; Mr. Benkt Linnander of Agema Infrared Systems; Mr. Stan LaBand of Amber; and Mr. Ken Lowe of FLIR Systems, Inc. is greatly appreciated.

Finally, many thanks are due to the Catherine and Amy, Lickety Split, and the innumerable people of the Coast Guard Auxiliary who provided their vessels and time to make the data collection possible.

ACRONYM LIST

AGC	Automatic Gain Control
CG	Coast Guard
FOV	Field of view
FPA	Focal Plane Array
FSI	FLIR Systems, Inc.
GPS	Global Positioning System
HgCdTe	Mercury Cadmium Telluride
InSb	Indium Antimonide
I/O	Inboard Outboard engine
IR	Infrared
LWIR	Long Wave Infrared
μ	micrometers
MRTD	Minimum Resolvable Temperature Difference
MWIR	Medium Wave Infrared
NETD	Noise Equivalent Temperature Difference
nmi	Nautical mile
OB	Outboard engine
PtSi	Platinum Silicide
R&D	Research and Development
RelHm	Relative Humidity
SIRIS	Shipboard Infrared Imaging System
SNR	Signal to Noise Ratio
VHF-FM	Very High Frequency, Frequency Modulated

CHAPTER 1

1.0 INTRODUCTION

1.1 PURPOSE

This report summarizes preliminary results of a field test conducted to evaluate the ability of an array of infrared (IR) sensor technologies to detect and classify potential law enforcement targets in the maritime environment. The field test was performed in Long Island Sound. The field test was conducted in late July in an effort to obtain IR data in hot and humid conditions that are similar to those experienced in the southeast United States and Caribbean waters (historical regions of high counter narcotics and immigration enforcement activity). The IR sensor array was established on the roof of the U.S. Coast Guard (CG) Research and Development (R&D) Center, Groton, CT, and was used to collect IR image data of target craft as they navigated through a predefined test scenario. Environmental data were collected at the sensor array and at the target vessel locations. A Global Positioning System (GPS) tracking system was used to track target vessels and to calculate an accurate distance between sensors and targets.

1.2 BACKGROUND

The CG R&D Center Surveillance Systems Branch has, over the years, endeavored to assimilate emerging technology advances into operations associated with various CG mission areas. In 1989, the R&D Center initiated a research effort that evaluated the benefits of providing an IR capability onboard CG vessels. This research led to the

decision to evaluate off-the-shelf IR technology for its utility in the shipboard environment. In 1994 the CG accepted delivery of the Shipboard Infrared Imaging System (SIRIS) and began a set of operational tests. The SIRIS incorporated a 512-by 512-element Platinum Silicide (PtSi) sensor with a specially designed set of optics to provide both narrow (2.8- by 2.2-degrees) and wide (11.7- by 9.2-degrees) fields of view. Initial review of these operational tests identified the benefits and limitations of this system. These are summarized in reference 1 (in review).

In concert with the SIRIS testing, the R&D Center reviewed the possibility of installing available shipboard IR systems onboard CG vessels of opportunity to conduct at-sea testing. Unfortunately difficulties were experienced matching CG operational facility schedules with the schedules of IR system vendors. This scheduling problem plus other similar problems allowed the R&D Center to postpone the IR field test and reevaluate project direction.

As an alternative approach, the R&D Center began a methodical review of available IR technology and ancillary equipment that would identify a set of minimum performance levels for a system that could detect, classify and evaluate target vessel activities from a Coast Guard cutter.

This project has been separated into three major tasks:

1. Review current technology associated with IR sensors and conduct a comparative evaluation of a representative sample of sensors,
2. Conduct a technology assessment of equipment related to the shipboard installation of IR equipment (e.g., stabilization platforms, range finders, trackers) and
3. Select a viable off-the-shelf system and conduct an at-sea evaluation to further qualify specifications for a potential CG procurement.

This report describes the process and preliminary results of the first phase of the project and begins to establish a set of criteria by which the CG may select an IR system for a future at-sea field test. It is organized into five chapters: chapter 1 discusses various aspects of the field test setup, including descriptions of the sensors and targets and an overview of the analysis procedures specifically developed in support of this effort; chapter 2 presents the analysis of the collected data; chapter 3 investigates image interpretation not related to resolution capabilities; chapters 4 and 5 present conclusions and recommendations based on field test results. The appendix provides an overview of IR phenomenology pertaining to the topics presented in this report. It is designed for the reader who is marginally familiar with IR sensors and the interpretation of IR images. Reference 2 provides a more detailed discussion of these topics and related IR phenomenology. Reference 3 provides a discussion of the LOWTRAN software used to model atmospheric transmission in this analysis.

1.3 FIELD TEST CONDUCT

This field test was conducted in Long Island Sound on a test range that stretched from the entrance buoys at the mouth of the Thames River in Connecticut, southward past the east side of Little Gull Island and out to safe water on the north side of Gardiners Island. Figure 1-1 depicts this test range.

A control station called R&D Control was established on the roof of the R&D Center at Avery Point that overlooked the test range providing a height-of-eye of approximately 80 feet. R&D Control operated the sensor array and maintained VHF-FM communications with the target vessels. Experiment design afforded real-time IR image data analysis while the data were being recorded. This analysis included recording detection and classification distances observed as well as documenting sensor ease of use

and image quality. In addition, R&D Control also maintained the official shore-side environmental data logs.

Target vessels met at buoy #2 at the mouth of the Thames River at the start of each data collection period. Environmental and radiometric data were recorded and the target vessels proceeded along the test range away from R&D Control. The target vessels stopped every half mile or at the direction of R&D Control, provided stern, beam, and/or bow aspects (as directed) relative to the location of R&D Control. Once data collection goals were met, R&D Control would notify all participants that the data collection was over and they could return to port. Table 1-1 provides a list of targets and their descriptions. The numeral in parentheses next to the vessel name denotes the assignment of an arbitrary target number used in the tables in chapter 2. Table 1-2 provides a summary of environmental conditions experienced during the field test based on surface vessel and R&D Control logs.

41°-20 N

This figure is a portion of
NOAA Chart 13205
Block Island Sound and Approaches

41°-10 N

072°-10 W

This chartlet not intended
for use in navigation.

Figure 1-1. Field Test Location

Table 1-1. Surface Vessel Target Summary

Vessel Name	Length (feet)	Width (feet)	Height (feet)	Construction
We Four (1)	23	8	8	Fiberglass I/O with full canvas sun cover and curtains
Radiant (2)	23	9.2	9	Fiberglass OB with hardtop and canvas curtains
Skipper II (3)	28	10	15	Fiberglass I/O with fly bridge and full canvas sun cover
Lickety Split (4)	25	7.5	30	Fiberglass with metal mast, nylon sail and small auxiliary OB
Catherine and Amy (5)	45	13	35	Wood with steel A-frame and <u>HOT</u> metal-exhaust stack
6-person life raft (6)	8.6	5.8	3.8	Rubber tubes with vinyl canopy

Table 1-2. Environmental Conditions Experienced

DATE*	TEMPERATURES (°C)			WIND		VIS (nmi)	ATM. PRES.	REL HM
	WATER	WET	DRY	VEL (KTS)	DIR (°T)			
17 July	**	20	22 to 23	calm	variable	10	29.93	60
18 July	19.5	21 to 22	22 to 24	calm	variable	3 to 7	29.78	70 to 83
19 July	19 to 20.5	20.5 to 22	25 to 29	5 to 10	210 to 270	8 to 12	29.85	46 to 68
20 July*	19 to 20	21.5 to 22.5	22	2 to 9	200 to 230	7 to 15	29.95	86 to 90
24 July	21 to 22	20.5 to 24	25 to 28	calm	variable	8 to 12	29.90	65 to 72
24 July*	19 to 20.5	20.5 to 21.5	21 to 23	calm	variable	7 to 9	29.93	86
26 July	20	23 to 23.5	24 to 25	7 to 10	180 to 190	1.5 to 3.5	29.94	83 to 85
26 July*	20 to 22	22.5 to 23.5	23 to 24	3.5	180 to 210	3 to 6	29.90	83 to 95
28 July	22	22.5 to 24	24 to 28	1.5 to 6	135 to 155	4	30.13	61 to 73

* night data collection periods.

** not available

1.4 IR SENSOR SYSTEM DESCRIPTIONS

The R&D Center obtained four IR sensors to support this field test: two that operate at LWIR wavelengths and two that operate at MWIR wavelengths. The sensors were chosen as a representative cross-sampling of the current state of technology for commercially available cooled IR systems. Table 1-3 summarizes sensor specifications and figure 1-2 depicts the sensor array used during the field test.

Table 1-3. Summary of Sensor Specifications

VENDOR MODEL	SPECTRAL BAND	DETECTOR TYPE	NETD (lens f/#)	WIDE FOV	NAR. FOV
Agema IR Systems Thermovision 1000	LWIR	5 X 1 element HgCdTe scanning array	< 0.2° (N/A)	7.0° by 5.0°	2.0° by 1.5°
FLIR Systems, Inc. SAFIRE	LWIR	4 X 4 element HgCdTe scanning array	< 0.1° (f/1.0)	28.6° by 16.8°	5.0° by 3.0°
Aerojet General Aerojet Thermal Imager	MWIR	640 X 480 element PtSi FPA*	< 0.15° (f/2.0)	12.3° by 9.13°	3.1° by 2.3°
Amber Radiance	MWIR	512 X 512 element InSb FPA*	< 0.025° (f/2.3)	7.41° by 7.41°	2.23° by 2.23°

*FPA - Focal Plane Array

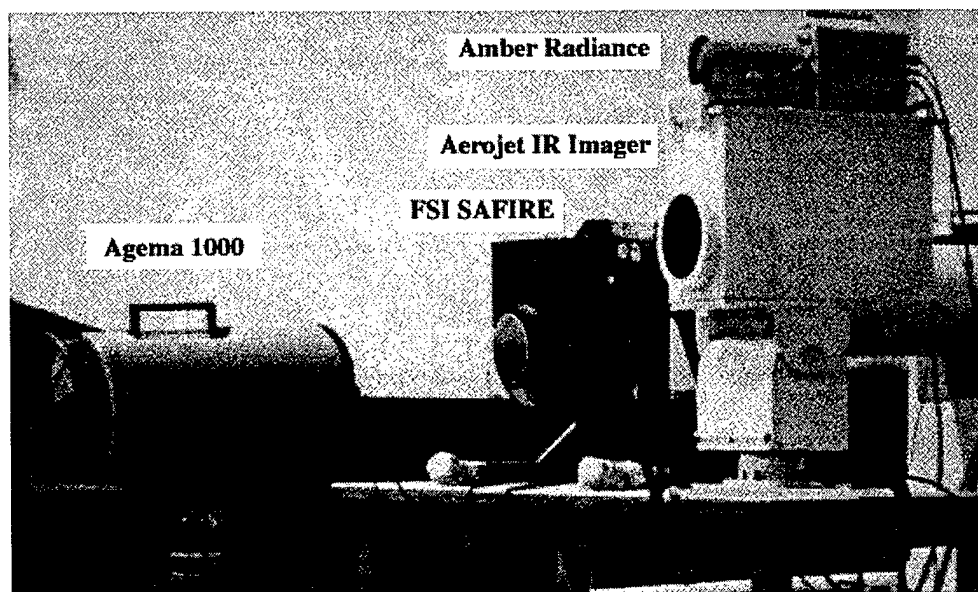


Figure 1-2. Sensor Array Used During July 1995 Field Test

1.4.1 LWIR Sensors

The two LWIR sensors selected were an Agema Infrared Systems Thermovision 1000 and a FLIR Systems, Inc. (FSI) SAFIRE. Sensor descriptions are provided below. Both systems incorporated an operator-selected menu system that permitted the alteration of the default conditions described below.

Agema Thermovision 1000

The Agema 1000 uses a cooled, five-element (linear) mercury-cadmium-telluride (HgCdTe) scanning array to provide a wide FOV of 7 by 5 degrees and a narrow FOV of 2 by 1.5 degrees. The system provides an electronic zoom of up to 8:1 that replicates pixels for image display. The enlarged image subtends a small portion of the FOV and allows the operator to pan within the FOV to view a desired object. The detector array scans the FOV to emulate a 565- by 376- element frame that is mapped to 798 by 400 pixel image available as RS-170, RGB, or S-video output.

The Agema 1000 is typically used in an installed, gimbal-mounted turret configuration. For this evaluation, the gimbaled turret was not necessary. Instead the sensor was mounted on a heavy-duty tripod for ease of aiming. A separate, hand-held remote control unit provided the operator with all required sensor adjustments and settings. An overlay filled the lower portion of the display screen. The overlay provided date and time, focus indication and a gain and level indication. It also indicated video polarity, live or still frame, frame filtering, and FOV selection. When operating the electronic zoom, a frame window appeared within the overlay to indicate the location of the enlarged image within the FOV. When operating in wide FOV, a narrow FOV size reticle framed the portion of the image available in the narrow FOV.

The sensor head contained connections for power, video output, and the hand-held controller. No external electronic processing unit was required.

FSI SAFIRE

The FSI SAFIRE uses a cooled, 16-element (4x4) scanning array to provide a wide FOV of 28.6 by 16.8 degrees and a narrow FOV of 5 by 3 degrees. The system provides a 2X electronic zoom that magnifies the center of the narrow FOV image. The detector array scans the FOV to create a 350- by 343-pixel frame that is available as a RS-170 video signal.

The SAFIRE was supplied in a gimballed three-axis turret. A separate, hand-held remote controlled both turret and sensor functions. Screen overlays included date and time, azimuth and elevation indicators, focus bar, gain and brightness bar, frame filtering, symbol selection mode, gain/level setting, stabilization mode, current FOV setting, and video polarity. When operating in the wide FOV, a narrow FOV size reticle marked the portion of the image included in the narrow FOV image. In addition, through a user-selected menu, a cross hair (graticule) could be turned on or off.

A central electronics unit connected the hand-held controller to the gimbal mount and sensor, provided video output ports, and controlled power to the system.

During this evaluation, difficulties were experienced with focusing the SAFIRE. Post-experiment diagnosis conducted by FSI indicated that a technical malfunction (worn/stripped focus travel screw) prevented the sensor from performing to its' full capability. General observations made here, will be investigated and documented during a follow-on demonstration of the sensor.

1.4.2 MWIR Sensors

The two MWIR sensors selected for the field test were an Aerojet General IR sensor and an Amber Radiance 1. Sensor descriptions are provided below.

Aerojet IR Sensor

The Aerojet IR sensor uses a cooled, 640- by 486-element Platinum Silicide (PtSi) focal plane array (FPA) to provide a wide FOV of 12.3 by 9.13 degrees and a narrow FOV of 3.1 by 2.3 degrees. The system provides a 2X electronic zoom that magnifies the center portion of either the wide or the narrow FOV image. Video output is provided as RS-170, with a parallel 12-bit digital output available.

The engineering prototype sensor provided for this field evaluation was mated to a remotely controlled pan/tilt pedestal to provide sensor pointing. Pan/tilt and sensor controls were operated through separate controllers. No screen overlays were available with the system.

A central electronics unit was connected to a power conditioner and to the sensor. It served as the sensor control unit and provided the RS-170 output used for this field test.

Amber Radiance 1

The Radiance 1 uses a cooled 256- by 256-element Indium Antimonide (InSb) FPA. For this field test, a dual objective lens (75- and 250-millimeter) was mounted on the camera to provide a 7.41- by 7.41-degree wide FOV and 2.23- by 2.23-degree narrow FOV. The detector array is mapped to a 512- by 464-pixel image window that is a portion of the 640- by 482-pixel full screen. Output is available as RS-170, RGB, S-video, or 12-bit digital video.

The Radiance 1 is configured for hand-held use with controls located on the sensor housing. An RS-232 connection on the rear of the sensor provides an interface for remote computerized control of the sensor. For this field test, the sensor was remotely controlled and a set of quick-access commands was created to eliminate the necessity of paging through software menu screens to modify the sensor configuration. Table 1.4 lists the commands and their results.

Table 1-4. Amber Radiance 1 Quick-Access Commands

COMMAND	RESULT
Full	Automatic gain control (AGC) based on full scene image
Mid	AGC based on center 50% of full scene image
Cent	AGC based on center 25 pixels within full scene image
Hor	AGC based on contrast at the major thermal horizon
OFF	AGC Off
Scope On	Line graph depicting pixel values across scene centerline on
Scope Off	Line graph depicting pixel values across scene centerline off.
NUC 1	Non-uniformity correction set for low contrast (hot scene).
NUC 2	<i>progressively longer integration time</i>
NUC 3	
NUC 4	Non-uniformity correction set for high contrast (cold scene)

A screen overlay was added to the left edge of the screen with the full image frame to the right. The overlay provided date and time, AGC status, mean analog-to-digital-counts (useful in optimizing integration time), contrast and brightness levels, non-uniformity correction setting, contrast enhancement table being used, color mode selected, and a live or frozen image indicator.

The Radiance 1 is essentially a self-contained unit, providing all control functions on the sensor housing. For the field test, the remote control (computer) interface was used. RS-170 and S-video output were routed to the video recording and display equipment.

1.4.3 Video Recording Setup

Figure 1-3 provides an image data flow schematic of the IR sensors, controls, and recording equipment. Figure 1-4 depicts the image data recorder workstation.

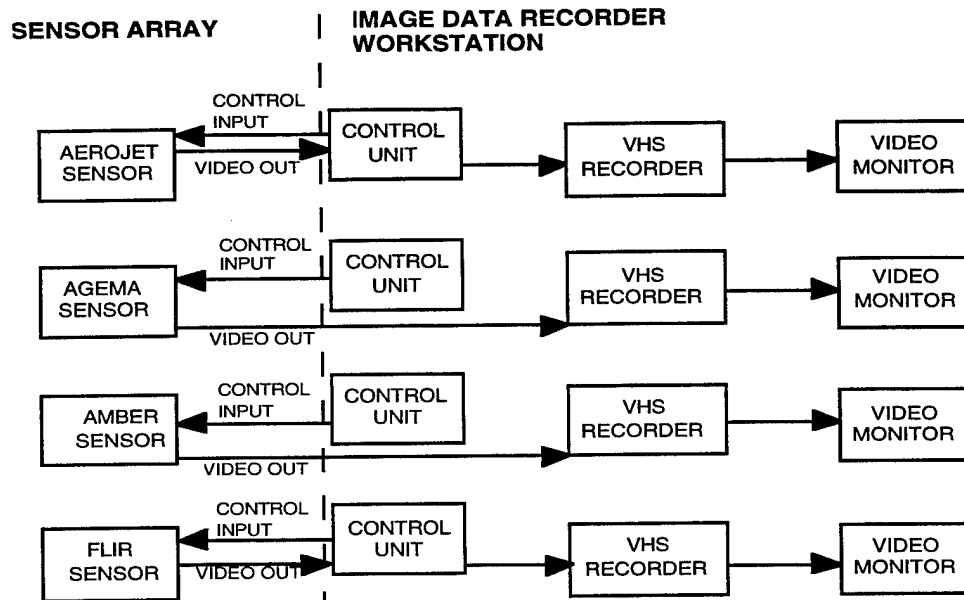


Figure 1-3. IR Data Collection System Schematic

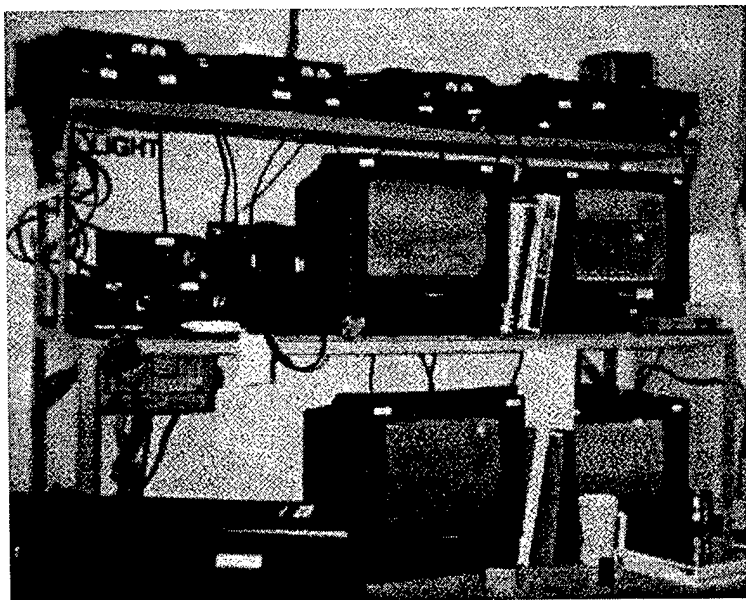


Figure 1-4. Image Data Recorder Workstation

1.5 TARGETS

The targets selected for this field test were limited to low-profile (small thermal contrast) surface vessels. Target vessels were selected to obtain data on a sampling of size, configuration and material. Table 1-1 provides a general description of the targets. Each vessel was chosen to represent a class of low profile targets of interest to the CG. Target materials were chosen to evaluate their detectability in the marine environment.

The life raft was the only target that did not have any self-generating heat source onboard; all other targets had personnel and/or engine exhaust. The F/V Catherine and Amy was the only target with a significant heat source exposed above the waterline; this was a 3-foot tall by 18-inch diameter exhaust stack located above the pilot house. All other sources of heat were well shielded (i.e., through hull) or were generated by target crews.

1.6 ANALYSIS PROCEDURE

This section describes the method selected for analysis of the collected data. Definitions of classification and detection distance are established to prevent or minimize skewness in the data collected, and to create repeatable and defensible results.

Empirical detection distance is defined as the farthest point at which a target still has sufficient thermal contrast to illuminate detector elements beyond the threshold of visibility for an alerted sensor operator. It is important to clarify the term alerted sensor operator. An alerted sensor operator has previous knowledge of where the target is and what it should look like. During this field test, the sensor operators watched the targets travel away from the sensor array and directed the target vessels to provide alternate profiles to increase the potential of detecting some aspect of the target. Marginal contrast, as yet undefined, in a few pixels is all that is needed for an alerted sensor operator to

maintain detection of the target. Given that the sensor is focused at the correct distance and is aimed in the correct azimuth as the target first becomes detectable, unalerted sensor operators will typically require greater target size and/or thermal contrast before acknowledging a detection.

Theoretical detection distance is determined by geometry of size and thermal characteristics of the scenario. For this evaluation, a target must subtend four detector pixels with sufficient energy contrast (signal) to be four times the NETD (noise) of the sensor (signal-to-noise ratio (SNR) of at least 4).

Empirical classification distance is defined as that distance at which a target can be classified into a predefined grouping (i.e., small pleasure craft, sailboat, fishing vessel). Operationally, this is a subjective measurement based on operator experience and whether or not the operator is alerted.

Several methods are available to calculate the **theoretical classification distance**. This paper proposes and justifies a modification to the Moser technique (reference 4). In essence, Moser stated that to classify a target at the 50-percent confidence level, 66 pixels of the detector array must be subtended. To classify a target at the 90-percent confidence level, a minimum of 115 pixels must be subtended. Theoretical classification distances provided in this report are based on this more stringent (90-percent level) criteria. The assumption is that at distances required to classify targets, the thermal contrast between the target and background is sufficient to energize detector array pixels.

The overriding requirement for calculating theoretical detection or classification distances is the availability of environmental data and target thermal data relative to the background. An atmospheric model known as LOWTRAN provides a measure of the transmission of a thermal signal through a specified atmospheric condition. The collected environmental data were the specified atmospheric conditions used for this evaluation. The transmission data were then used to determine if the thermal signal contrast at the sensor

and number of pixels subtended by the signal met classification and/or detection criteria. Successive iterations were calculated until theoretical detection and classification distances were obtained for each set of conditions experienced.

The empirical distances reported in the following sections are based on the time and position plots generated from the surface targets GPS tracking unit. For post experiment analysis, computer generated target vessel track plots were generated. These plots and an accompanying list of GPS time and position data enabled the analysis team to measure the distance from the GPS position of the targets to the GPS position of the sensor array. The R&D Control logs were reviewed, while watching the recorded video, to confirm the time and position of the observed detection and classification distances. The times from each detection or classification were compared to the plots and listed GPS time and position sheets to obtain the distance. In cases where the detection or classification were deemed marginal by the data recorders during the field test, that position is included in the determination of farthest distance for this report.

As has been described, a much more stringent criteria has been set for theoretical distances presented here than has been set for the empirical distances. The field test measured an alerted operator's ability to observe the targets and the theoretical model attempts to predict detection performance of an unalerted operator. The final report will establish the distance at which the video data most closely resembles the criteria for the theoretical distances. Reference 5 presents a review of a sample data set using this more stringent criteria for empirical data.

BLANK

CHAPTER 2

2.0 DATA ANALYSIS

This section contains the results of the analyses described in chapter 1. Empirical detection and classification distances are summarized. Theoretical detection and classification distances are determined for one daytime and one nighttime data collection period and compared to the empirical distances determined for that test period. A comprehensive final report using the results presented here will be developed and promulgated at the completion of this project.

2.1 EMPIRICAL DETECTION AND CLASSIFICATION DISTANCES

The real-time image analysis conducted during the field test was verified in a post-test review of the recorded image data and compared to time/date-correlated plots. Distances provided are based on the difference of the GPS position at the sensor array and the GPS-equipped target vessel when the targets were directed to provide alternative aspects to R&D Control.

2.1.1 Empirical Detection Distances

Detection distance is the range (in nmi) when a target was barely perceptible against the background. For this evaluation, the beam aspect displayed the largest target surface area and typically resulted in the farthest detection distance. Table 2-1 summarizes detection distances obtained by each sensor during each data collection period. These detection distances indicate the farthest distance from which the target was detected with each sensor. Those values preceded by a "greater than" symbol (>) were detected at that distance and the test period was terminated prior to determining if the target could be detected beyond that distance. Data in table 2-1 presented for the daytime data collection period on 24 July include wide FOV/narrow FOV empirical detection distances.

Table 2-1. Empirical Detection Distances (nmi)

DATE	TIME	TARGET	SENSOR			
			AEROJET	AMBER	AGEMA	FSI
17 JULY	1330-1500	1	>4.2	>4.2	>4.2	2.9
18 JULY	1330-1530	3	4.0	>4.5	4.5	2.4
		5	>6.7	>6.7	>6.7	2.4
19 JULY	1330-1700	1	5.8	>7.9	5.5	2.9
		4	>6.3	>6.3	5.5	2.9
		6	5.9	>6.3	5.0	2.3
20 JULY*	2100-2300	2	6.9	6.9	4.4	4.0
		4	6.9	6.9	4.4	3.5
24 JULY	1330-1600	1	3.1/9.6	4.6/9.6	3.1	1.7
		4	4.6/9.6	5.1/9.6	3.7/5.4	2.0
24 JULY*	2100-2300	1	5.0	5.6	2.7	2.4
		4	5.0	5.6	2.7	1.4
		6	4.0	4.0	2.4	1.4
26 JULY	1300-1500	1	3.9	4.4	3.9	3.4
		5	>=8.2	>=8.2	4.4	3.8
26 JULY*	2100-2200	2	2.9	3.4	2.8	2.4
		5	3.9	4.4	3.9	2.8
28 JULY	1100-1215	6	4.3	4.3	4.0	>0.4

* Nighttime data.

2.1.2 Empirical Classification Distances

Classification distance is the range (in nmi) immediately before R&D Control could no longer place or classify the geometric form into one of the target classes in table 2-2. For these data, the beam aspect displayed the most significant target profile and resulted in the farthest classification distance. Table 2-3 summarizes classification distances obtained by each sensor during each data collection period. Those values preceded by a "less than" symbol (<) were unable to be classified at the distance where the targets commenced the day's data collection period.

These classification distances do not necessarily meet the criteria of 115 pixels subtended as stated in section 1.6, rather they present the classification distance established by alerted operators during the actual field test and include subjective data. Further analysis should be conducted before the final report is published to limit these distances to the 115 pixels required for the 90-percent confidence level.

Table 2-2. Target Classification Profiles

CLASSIFICATION	CHARACTERISTICS
Small Pleasure Craft	Low profile with raised fore/midcabin and sun cover*
Small Sailboat	Low profile with triangular sail*
Fishing Vessel	Low profile with deck house and outrigger masts.

* Note - sail and sun cover may not always be detectable in IR.

Table 2-3. Empirical Classification Distances (nmi)

DATE	TIME	TARGET	SENSOR			
			AEROJET	AMBER	AGEMA	FSI
14 JULY	1100-1400	1	NO DATA TAKEN			
17 JULY	1330-1500	1	3.8	3.8	3.8	<1.5
18 JULY	1330-1530	3	2.0	2.0	2.0	<1.6
		5	2.9	3.4	3.4	<1.6
19 JULY	1330-1700	1	2.9	2.9	2.9	<1.4
		4	5.0	5.0	5.0	1.7
		6	<1.4	<1.4	<1.4	<1.4
20 JULY*	2100-2300	2	2.4	2.4	1.5	<1.5
		4	4.9	4.4	4.0	1.9
24 JULY	1330-1600	1	<1.5	<1.5	<1.5	<1.5
		4	1.7	2.0	2.0	<1.5
24 JULY*	2100-2300	1	2.4	2.4	1.4	1.4
		4	4.4	4.4	1.4	1.4
		6	<1.4	<1.4	<1.4	<1.4
26 JULY	1300-1500	1	2.4	2.4	2.4	<1.5
		5	2.9	2.9	2.9	1.5
26 JULY*	2100-2200	2	2.4	2.9	1.9	<1.5
		5	2.4	2.9	2.4	1.5
28 JULY	1100-1215	6	>0.4	>0.4	>0.4	>0.4

* Nighttime data.

2.2 THEORETICAL DETECTION AND CLASSIFICATION DISTANCES

For this report, one daytime and one nighttime data collection period were selected for the calculation of detection and classification distances. The remaining data will be analyzed and presented as part of the final report due in the spring/summer of 1996. Due to the technical malfunction noted in section 1.4.1, FSI SAFIRE theoretical distances have not

been calculated. More detailed analysis of the effect of the focus malfunction should precede documentation of its comparative performance.

The daytime test period from 17 July 1995 and the nighttime test period from 24 July 1995 were selected because they represented the most consistent radiometric and environmental conditions obtained. The 23-foot pleasure vessel WE FOUR and the 25-foot sailboat LICKETY SPLIT were used as targets during these test periods.

The calculated detection and classification distances are considered maximum theoretical distances at a 90-percent confidence level. Inaccuracies measuring environmental data or target thermal contrast can result in theoretical distances that are significantly longer or shorter than those obtained in the field.

2.2.1 Theoretical Detection Distances

Following the principles outlined in section 1.6, detection distances were calculated for the selected daytime and nighttime data collection periods. Table 2-4 provides these distances. Under the environmental conditions experienced during the 24 July test period, the detection distance estimates predict that the MWIR sensors should outperform the LWIR sensors. At approximately three nmi, atmospheric attenuation is predicted to prevent these targets from being detectable with the LWIR sensors used. The difference in sensitivity between InSb and PtSi detectors is also evident (Amber detection distance during the day of 24 July for the WE FOUR is calculated to be approximately 2.5 nmi longer than the Aerojet detection distance). Of note for this report is that the frame rate for the Amber sensor is twice that for the other sensors. Analysis continues to be conducted to determine the full impact of the increased frame rate on sensor sensitivity.

Calculation of detection distances for the nighttime data collection period was far less complex than for the daytime data collection period. At night, the thermal scene remains fairly consistent. Thermal contrast at the target site can be measured and assumed to remain the same for a long enough period of time to make calculated contrast at the

sensor meaningful. The thermal contrast at the sensor can be compared to the NETD, and a valid determination of detectability can be made. The complexity of the daytime scene, with reflected solar energy and solar warming contributing to the scene, makes calculating detection distance far more difficult, especially in the MWIR spectrum. Sun angle, the angle of the reflective surfaces of the target, reflectivity of the background, absorption and emission of solar energy by the target and background, must all be considered or be assumed negligible. Figure 2-1 provides a pictorial representation of the thermal scene. Figure 2-2 demonstrates the fundamental procedure behind the theoretical calculations.

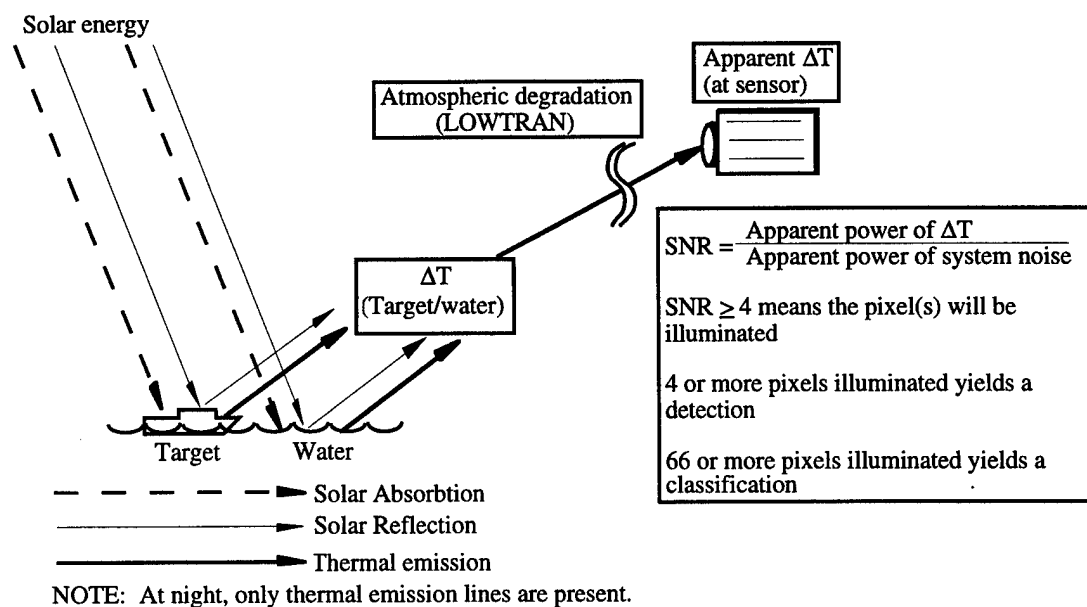


Figure 2-1. Simplified Thermal Scene

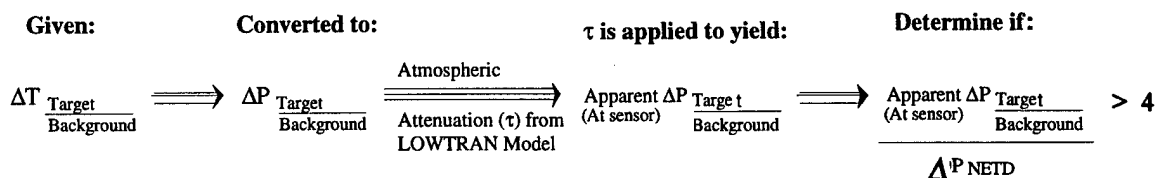


Figure 2-2. Fundamental Procedure Behind Theoretical Calculations

Nighttime detection distances are provided in table 2-4. Daytime detection distances are still being determined. Because the greatest gains obtained by using IR sensors is obtained in nighttime or poorly illuminated conditions, daytime detection distances are not considered essential for this report.

2.2.2 Theoretical Classification Distances

Following the principles outlined in section 1.7, classification distances were calculated for the selected daytime and nighttime data collection periods. Table 2-5 provides these distances. Under the environmental conditions experienced, the classification distance estimates indicate that classification distances for the three two-degree-FOV sensors should be approximately the same. At these shorter distances, the environmental conditions should not appreciably attenuate the LWIR signal to decrease detectability beyond the geometric size-limiting. Because of this, daytime and nighttime theoretical classification distances are the same for the WE FOUR. The differences between theoretical classification distances for the WE FOUR and LICKETY SPLIT are a result of the sailing vessel's larger surface area and distinct appearance of the sail.

Table 2-4. Theoretical Detection Distances (nmi)

DATE	TARGET	SENSOR		
		AEROJET	AMBER	AGEMA
17 JULY	WE FOUR	TBD	TBD	TBD
24 JULY*	WE FOUR	5.0	7.5	3.0

* Nighttime data.

Table 2-5. Theoretical Classification Distances (nmi)

DATE	TARGET	SENSOR		
		AEROJET	AMBER	AGEMA
17 JULY	WE FOUR	2.2	1.7	2.4
24 JULY*	WE FOUR	2.2	1.7	2.4
	LICKETY SPLIT	4.0	3.0	4.4

* Nighttime data.

2.3 CORRELATION OF EMPIRICAL AND THEORETICAL DISTANCES

The theoretical distances should be viewed as a maximum theoretical distance at the 90-percent confidence level. Empirical distances were more subjective and should be considered the farthest distance an alerted operator can either detect contrast or to distinguish marginal target features. When subjected to the same criteria, theoretical distances can be expected to be longer than empirical distances because actual sensor performance is subject to improper sensor tuning, aging detectors, varying environmental conditions, and the like. Because empirical distances presented here are subject to a less stringent requirement (less than 115-pixels for the 90-percent confidence level), they are expected to be equivalent to or slightly longer than the theoretical distances.

2.3.1 Correlation of Detection Distances

Nighttime detection distances for the WE FOUR are compared in table 2-6. The theoretical detection distance for the Aerojet sensor is within one-half nmi of the empirical detection distance. The theoretical detection distance for the Amber sensor is roughly two miles longer than the empirical detection distance. The theoretical detection distance for the Agema sensor is also within one-half nmi of the empirical detection distance (the distance between documented pauses for R&D Control review). Calculated detection distances for the Aerojet and Agema sensors agree with empirical findings. The theoretical and empirical detection distances for the Amber sensor do not agree sufficiently to indicate that a proper correlation exists. These calculations will be reviewed and developed for the final report.

Table 2-6. Comparison of Empirical and Theoretical Detection Distances

		DETECTION DISTANCES EMPIRICAL / CALCULATED		
DATE	TARGET	Aerojet	Amber	Agema
17 JULY	WE FOUR	TBD	TBD	TBD
24 JULY*	WE FOUR	5.5 / 5.0	5.6 / 7.5	2.7 / 3.0

* Nighttime observations.

2.3.2 Correlation of Classification Distances

Classification distances are compared in table 2-7. Daytime empirical classification distances were always longer than the corresponding theoretical classification distances. It is likely that this is due to the thermal warming of the canvas bimini top. MWIR sensor empirical classification distances were always longer than the corresponding theoretical classification distances. The Agema sensor provided shorter nighttime empirical classification distances than the corresponding theoretical classification distances.

Reference 5 documents a study that was more focused on the WE FOUR during these particular periods and included a more stringent criteria for empirical classification distance. Empirical distances presented above are based on the alerted observer watching for a particular target feature while those of reference 5 required that the feature be recognizable with more confidence. It should be noted that the empirical distances obtained during the field test resulted in targets subtending 60 to 80 pixels, while the more stringent criteria resulted in targets subtending 110 to 120 pixels (closely matching the theoretical criteria established). Reference 5 indicated a strong correlation exists between theoretical classification distances and the more stringent empirical determination of classification. The final report will report empirical classification distances based on this more stringent criteria.

Table 2-7. Comparison of Empirical and Theoretical Classification Distances

		CLASSIFICATION DISTANCES EMPIRICAL / CALCULATED		
DATE	TARGET	Aerojet	Amber	Agema
17 JULY	WE FOUR	3.8 / 2.2	3.8 / 1.7	3.8 / 2.4
24 JULY*	WE FOUR	2.4 / 2.2	2.4 / 1.7	1.4 / 2.4
	LICKETY SPLIT	4.4 / 4.0	4.4 / 3.0	1.4 / 4.4

* Nighttime observations.

BLANK

CHAPTER 3

3.0 INVESTIGATION OF NON-RESOLUTION-RELATED IMAGES

Chapter 2 addressed the primary objectives of this report, which were to summarize data collected during the July field test and to examine detection and classification distances associated with the IR sensors evaluated during the field test. This chapter presents and discusses ancillary issues relating to IR sensor performance that were documented during the field test. The quality of images in the figures presented in this report is degraded from the full motion video due to the process of capturing the frame and reproduction of the report.

3.1 SUN GLINT

As discussed in appendix A, reflected solar energy introduces more scene noise in the MWIR spectrum images than in the LWIR spectrum images. In brightly sunlit conditions, the sensor array recorded some of the effects. Figures 3-1 and 3-2 present images of the target vessel LICKETY SPLIT on 19 July 1995. The images were recorded at 1336 local time on one of the clearest and brightest days of the field test. Target detection was considered marginal at 1.4 nmi with the MWIR sensors due to interference from reflected solar energy, while the LWIR sensors did not suffer from the reflected solar radiation. As the test progressed and the sun moved across the sky, sun glint was minimized and target contrast improved in the MWIR images. At narrow FOV detection distances, sun glint was negligible and the MWIR sensors benefitted from reflected solar energy. Tilting of the flat horizontal and vertical target surfaces due to pitch and roll resulted in the reflected solar energy regularly being directed toward the sensor array and had the appearance of a signal mirror reflecting visible energy. The maximum detection distances achieved were 9.6 nmi with the MWIR sensors and 5.4 nmi with the LWIR sensors.

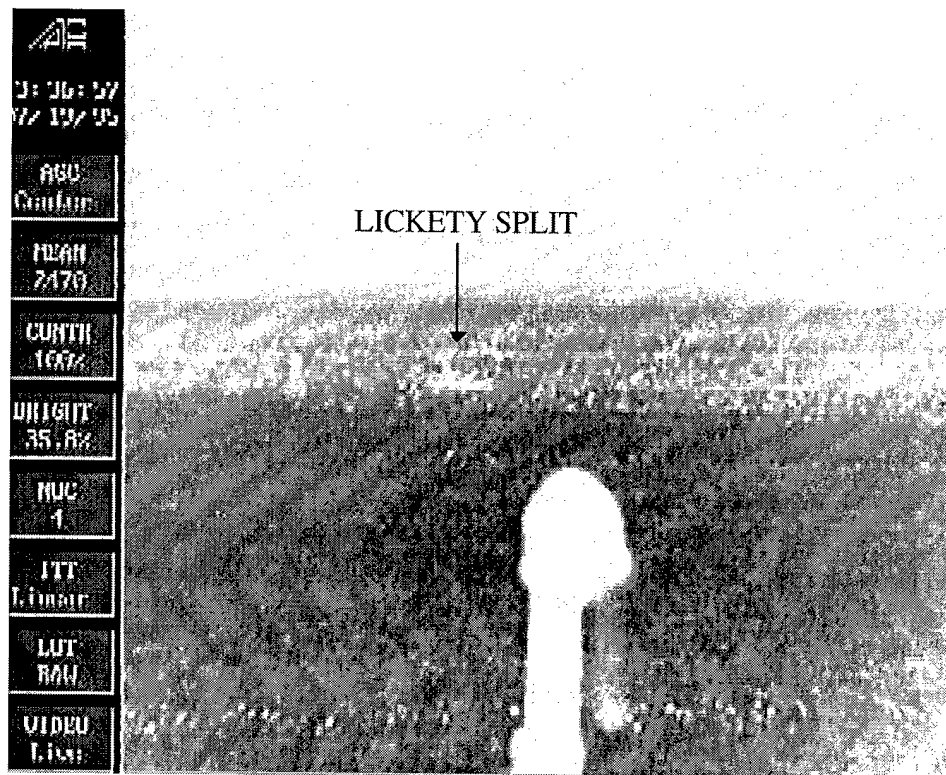


Figure 3-1. MWIR Image of the LICKETY SPLIT Showing Sun Glint

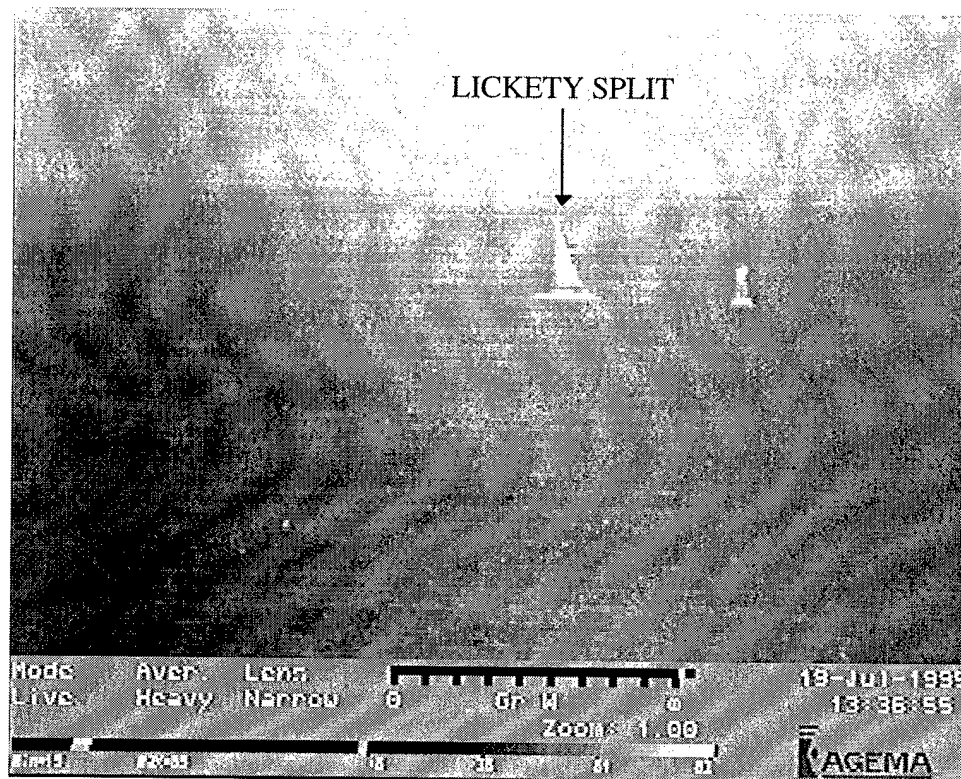


Figure 3-2. LWIR Image of the LICKETY SPLIT During Period of MWIR Sun Glint

3.2 TRANSITION PERIODS

An IR transition period is defined as the period of time when the IR scene is cooling (night) or warming (morning) such that objects within the scene are transitioning, radiometrically, from cool to warm (or vice versa) relative to the background. This phenomenon was observed when sun glint dominated the scene and during the earlier portions of the nighttime test periods that included an unheated target (i.e., sail or life raft). Figure 3-3 provides an excellent representation of what occurs during a thermal transition period. The image was recorded at approximately 1215 local time on 20 July 1995. The bottom of the sail is visible (warm) against the water background, but the top portion of the sail cannot be discerned from the warmer sky background. The sail and water will cool as the night progresses and, depending on air temperature (the major surface contact of the sail), the sail may become cooler than the water. When the sail is radiometrically the same temperature as the background, it will be undetectable to the IR sensor.

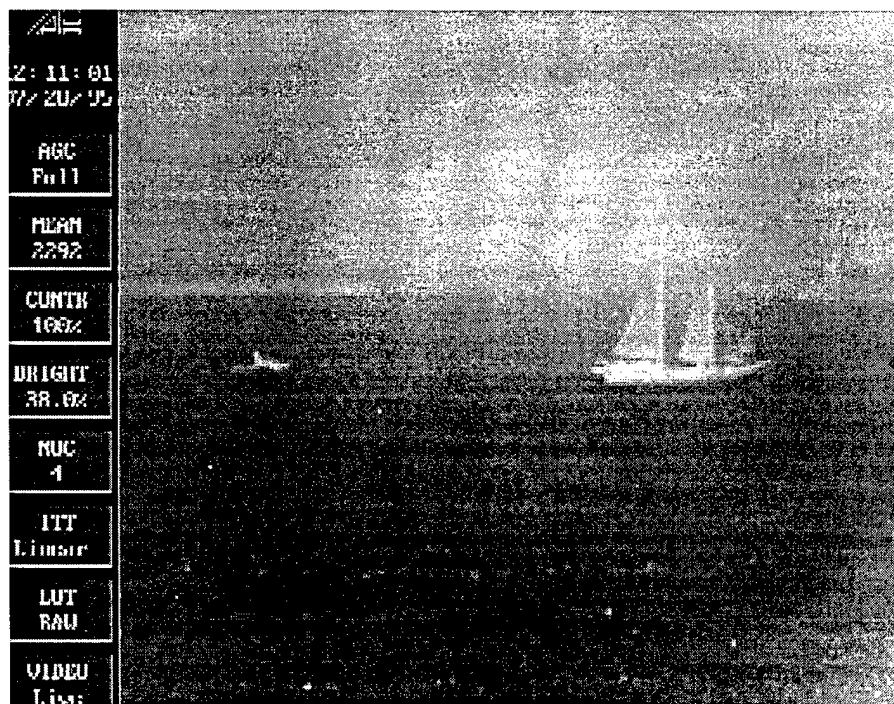


Figure 3-3. Representation of Thermal Transition

Figures 3-4 through 3-7 provide additional documentation of IR transition phenomena. Figures 3-4 (LWIR) and 3-5 (MWIR) depict the sailboat LICKETY SPLIT, pleasure boat WE FOUR and 6-person liferaft during daytime data collection on 19 July. The difficulty discussed in section 3.1 with sun glint is obvious in these images. In the LWIR image, all three targets appear warmer than the background. Review of LWIR video from other data collection periods indicates that target materials consistently appeared warmer than the water background during daytime imaging. In figure 3-5, the WE FOUR and liferaft (right-hand targets) appeared warmer than the background. The hull of the WE FOUR is not clearly defined and is not as warm as the bimini top. The hull of the LICKETY SPLIT was typically warmer than the background, but marginally so. The sail frequently transitioned from warmer than the background to nearly neutral as depicted in figure 3-5. Sun angle and the motion of the sailboat had much to do with the appearance (warm or cool) of the sail in the MWIR scene. The difference between the sail and the life raft depicted in figure 3-5 can be attributed to the darker material of the life raft absorbing more solar energy and the closed life raft trapping heat inside.

Nighttime imaging of these targets on 24 July yielded nearly identical image data for the sailboat (sail) and life raft targets. In figures 3-6 and 3-7 the WE FOUR can be seen to the right of the LICKETY SPLIT. Between the two, being towed by the WE FOUR is the 6-person liferaft. The sail and liferaft are marginally detectable, even at this relatively close distance (1.5 nmi) with the MWIR sensors. The LWIR sensors, on the other hand, clearly depict both as cooler than the background. The MWIR image depicts radiometrically warm fiberglass hull materials and the LWIR image depicts radiometrically cool fiberglass hull materials. Neither the sail nor the life raft were subjected to daytime differential heating and, therefore, emissivity differences account for the major radiometric differences between these targets.

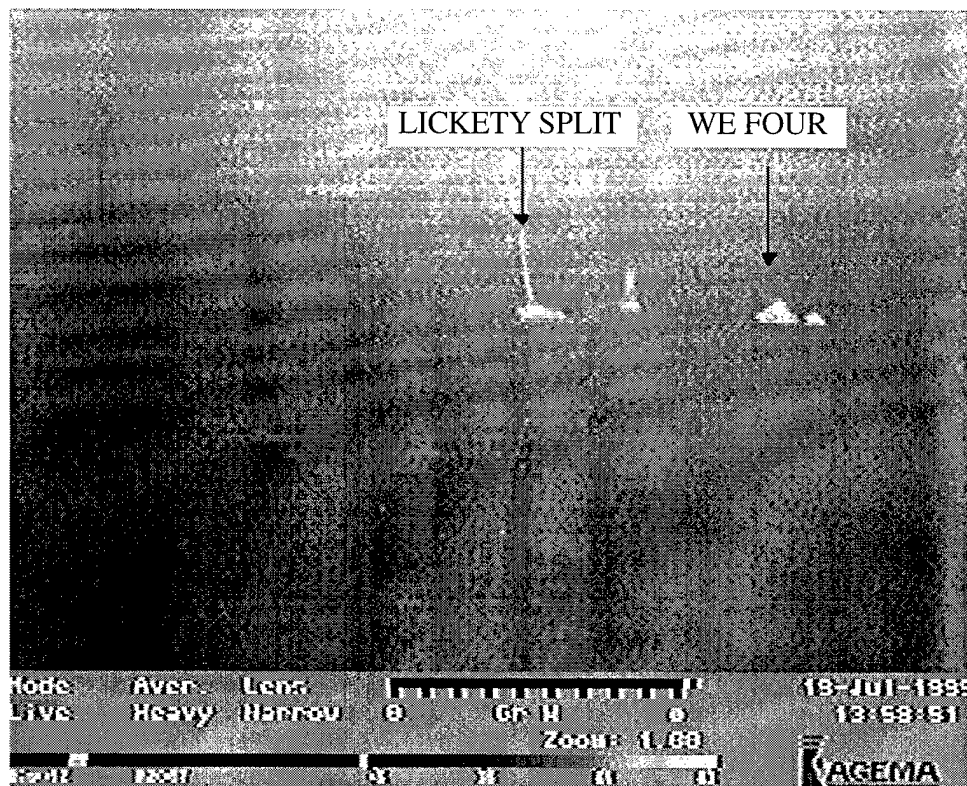


Figure 3-4. LWIR Daytime Image of Targets, 19 July 1995



Figure 3-5. MWIR Daytime Image of Targets , 19 July 1995

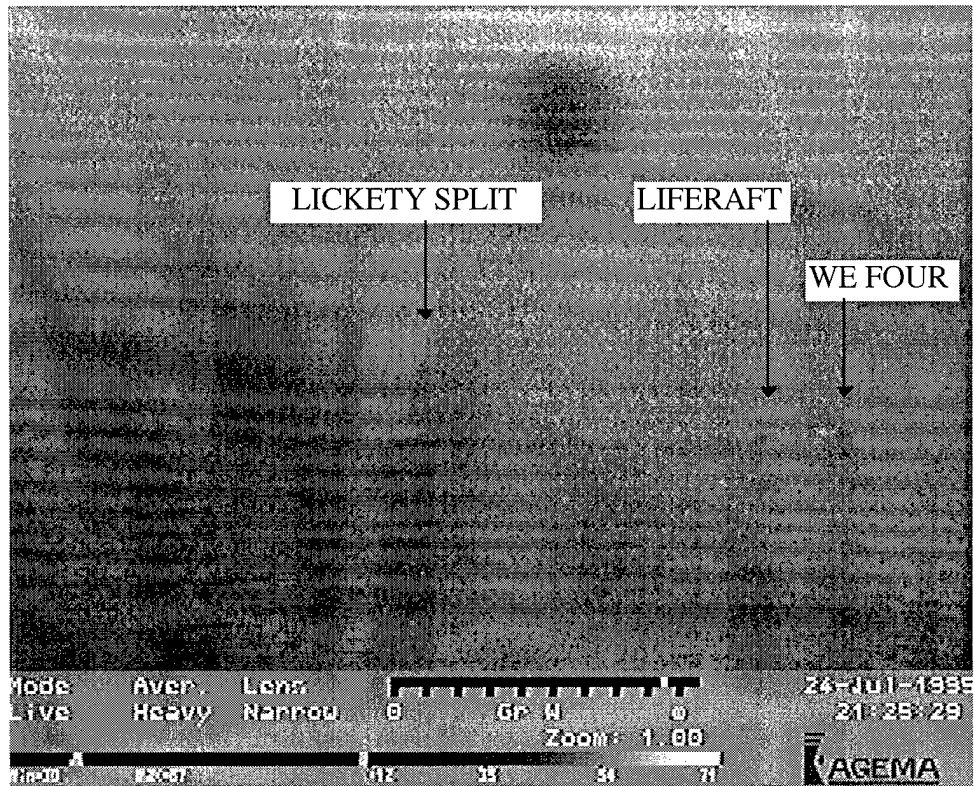


Figure 3-6. LWIR Nighttime Image of Targets, 24 July 1995

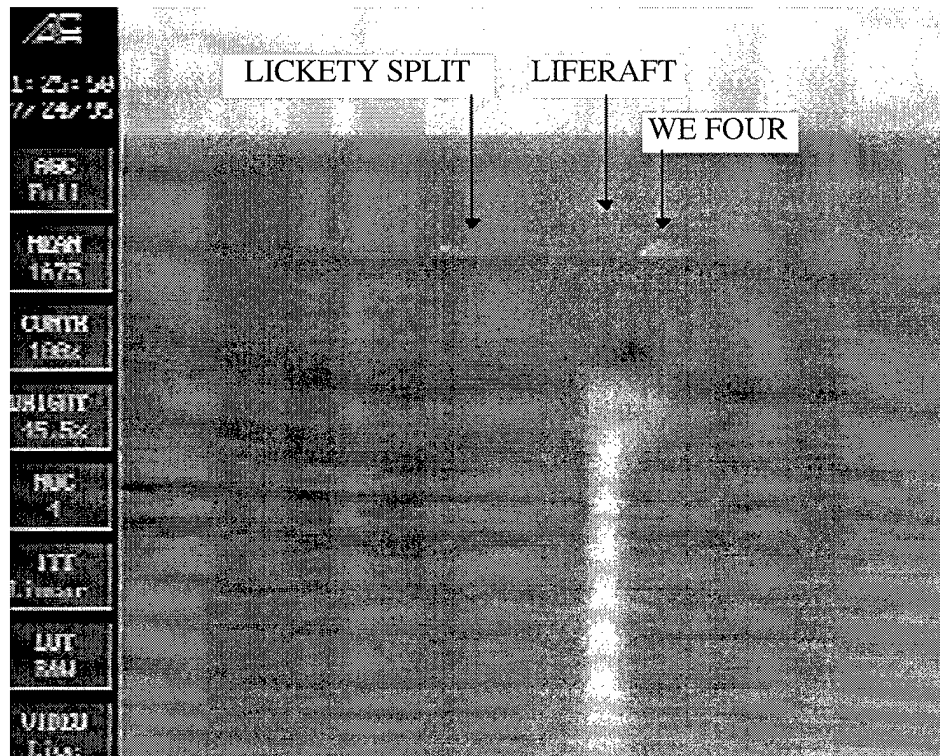
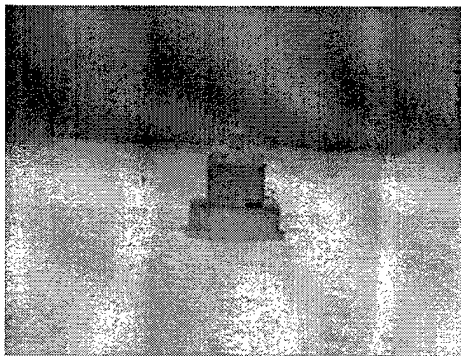


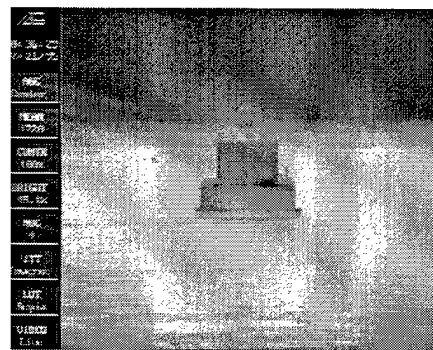
Figure 3-7. MWIR Nighttime Image of Targets, 24 July 1995

3.3 VIDEO POLARITY

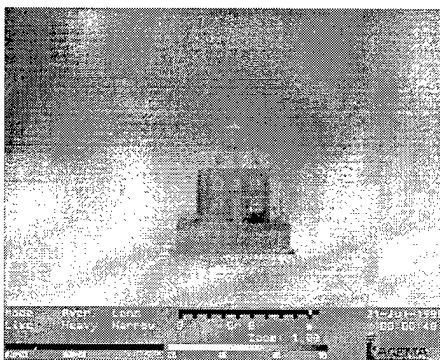
All four sensors provided the capability to represent the video image in black = hot or white = hot video polarity. In addition, the Agema and Amber sensors provided several false color modes. Figures 3-8 and 3-9 depict black = hot and white = hot images of Ledge Light during the night on 20 July. False color modes were examined for those systems that offered that capability, but due to the format of this report, they are not represented here. Upon comparison of image content, no difference was found between white = hot, black = hot, and colorized video representation. It appears that video polarity or false coloring is a matter of operator preference.



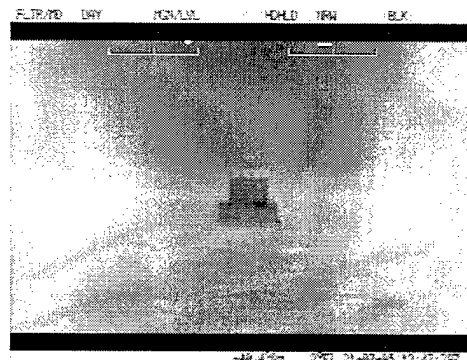
a. Aerojet General



b. Amber Radiance 1



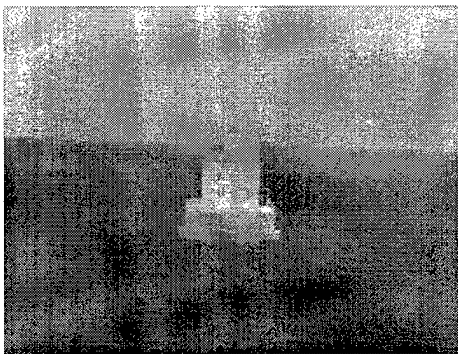
c. Agema Thermovision 1000



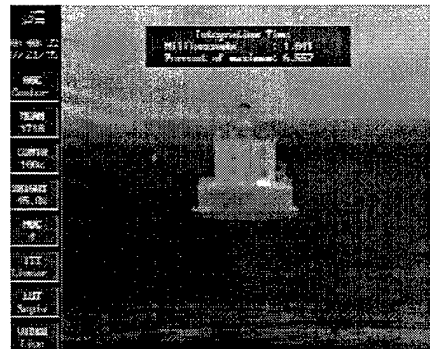
d. FLIR Systems SAFIRE

Figure 3-8. Black = Hot Video Polarity from All Sensors

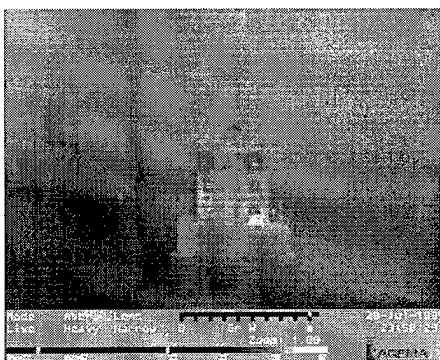
All sensors arrived with white = hot set as the default video polarity. This indicates that vendor experience is that operators prefer that video polarity. During this field test the majority of imaging was also done in white = hot video polarity. Examining reasons for this preference provides several examples that could condition the human mind. The sun is bright and hot while the dark night sky is cold, a burning light bulb is hot but cools when turned off or burnt out, cold steel can be heated until white hot, and so forth. Although these examples indicate a bias toward this video polarity, the reverse video polarity can improve video presentation under certain conditions, and should not be eliminated from systems containing the option.



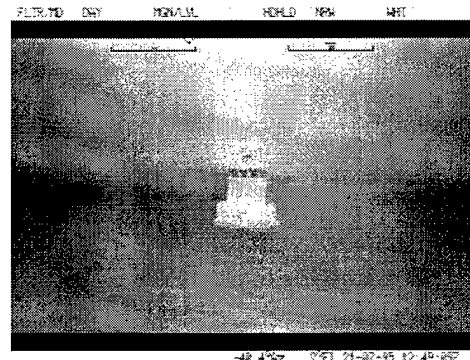
a. Aerojet General



b. Amber Radiance 1



c. Agema Thermovision 1000



d. FLIR Systems SAFIRE

Figure 3-9. White = Hot Video Polarity from All Sensors

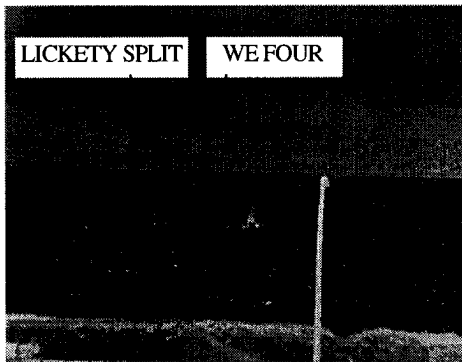
3.4 WIDE FIELD OF VIEW

Although the change between wide FOV and narrow FOV is clearly a resolution issue, the goal for any system is to maximize the detection and classification distances. Since the wide FOV yields shorter detection and classification distances than the narrow FOV counterpart, discussion of wide FOV characteristics that would have been distracting in chapter 2 are discussed here.

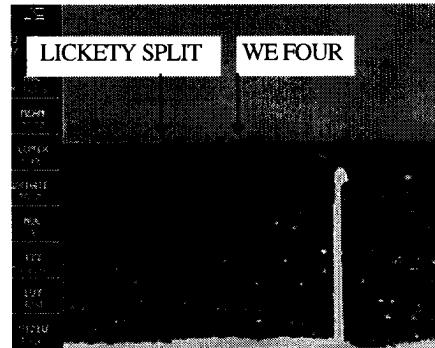
As shown in table 1-3, there was a broad range of wide FOV optics. Figure 3-10 depicts similar views of the test range with target vessels at 1.5 nmi during the day of 24 July.

In these images it was apparent that detection and classification distances were limited by the resolution provided with these FOVs; other images collected using the wide FOV corroborate this. The target vessels WE FOUR and LICKETY SPLIT are indicated by arrows in each of the images. R&D Control personnel commented that the narrower-wide FOV provided by the Agema 1000 presented the most useable information for the distance and targets used during this field test.

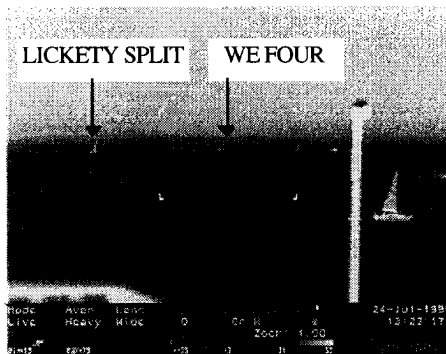
Another factor contributing to the decrease in target detectability was sunglint. In wide FOV images, in comparison to narrow FOV images, a target subtends fewer pixels within the region of sun glint and is not as readily detected. The Aerojet image in figure 3-10 most clearly demonstrates this. Without prior knowledge or the opportunity to view the full motion video, the WE FOUR is only marginally detectable in the sunglint.



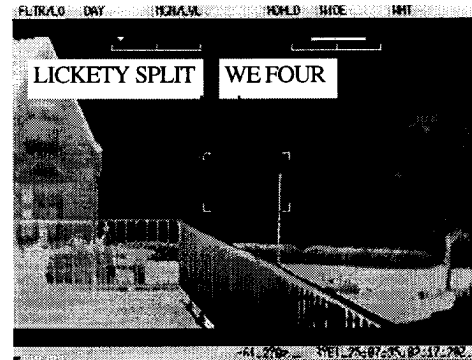
a. Aerojet General



b. Amber Radiance 1



c. Agema Thermovision 1000



d. FLIR Systems SAFIRE

Figure 3-10. Demonstration of Wide Field of View from All Sensors

3.5 GENERAL IMAGE DATA AND SENSOR PERFORMANCE

Several operationally significant aspects of image data and sensor performance became evident during this field test and post-test review.

Image Data

- The bimini sun cover on the WE FOUR was dark green material that became very hot during daytime data collection periods. At night, the bimini top was notably less detectable to the IR sensors.

- The Agema 1000 presented a well-contrasted image of scene information out to the target detection distance. However, with the atmospheric conditions experienced during this test period, image detail was absent beyond the target detection distance. Although hampered by a technical malfunction, the FSI SAFIRE image data demonstrated a similar trait.

- During this field test the LWIR sensors were considerably less affected by scene clutter than the MWIR sensors, especially during periods of high sun glint. However, they also suffered from a loss of thermal signal (due to atmospheric attenuation) over the longer distances desired for detection and classification.

- Small targets, such as lobster buoys, were detectable by the MWIR sensors out to approximately a mile during daytime data collection periods. LWIR sensors were less likely to detect these small targets. With no radiometric information, it is assumed that the same condition that produces sun glint in the MWIR (better solar energy reflection) resulted in better detection conditions for these objects during periods where sun glint did not dominate the scene. Neither MWIR nor LWIR sensors detected the lobster buoys during nighttime data collection periods. Again there are no radiometric data available; however, a reasonable assumption is that the emissivity differences between the buoy and background are not sufficient considering the pathlengths required.

Sensor Performance

- During a post-experiment system check, FSI engineers confirmed that focus problems experienced during this field test were the result of mechanical problems within the sensor housing. Actual SAFIRE performance can be expected to be better than that experienced during the field test. However, poorer scene detail resulting from the SAFIRE's much wider FOV is expected to mirror results obtainable with a properly operating system.

- The Aerojet sensor's display monitor output had a noticeable flicker. The flicker was quite bothersome in the darkened video data collection room. Aerojet engineers could not identify the source of the flicker during phone conversations held while the field test was being conducted.

- The video filter and 2x zoom controls were located on the same toggle switch for the Aerojet sensor. At times, the video filter significantly enhanced video presentation, and the 2x zoom image could be improved by the ability to filter the enlarged image.

- The Aerojet detector calibration cycle generated a random pattern that was often left as a shadow on the screen. At times, the detection of small or weak targets was more difficult because of the residual pattern.

- The ability to control the Amber sensor with a computer provided precise control of the sensor. However, some experience was required to become familiar with this computer control which would be impractical for shipboard employment. Each participating sensor vendor agreed that a specific controller could easily be provided with those features required to support the CG mission area.

- Although vendors have developed several ways to protect the front lens when not in use, stowing the lens face within the turret housing, appears best for shipboard installation.

CHAPTER 4

4.0 CONCLUSIONS

Only a preliminary analysis of the field test results have been presented. Additional calculations for detection and classification distances and more detailed analysis of captured image detail will be combined with the evaluation of ancillary equipment in the final report. Conclusions based on the results of the field test are summarized below.

- The use of a single set of theoretical calculations or empirical measurements to describe IR sensor detection or classification capabilities lends itself to misinterpretation. The interaction of target and sensor characteristics with the non-static nature of environmental factors is very dynamic and constantly alters detection and classification distances. Any review of sensor performance must be viewed as dependent on conditions. Actual results are also operator dependent.

- The environmental conditions during this field test caused LWIR sensors to experience an atmospheric transmissivity "curtain" that obscured targets approximately 1 nmi beyond the maximum classification distance.

- MWIR sensors did not experience, due to the field tests humid conditions, the signal loss that the LWIR sensors experienced and consequently, provided significantly longer detection distances.

- High sun angles on clear days caused a significant amount of sun glint in the MWIR image. This sun glint adversely affected imaging conditions in large portions of the FOV from one to one and a half hours on either side of peak sun elevation. Previous research conducted by or for the U.S. Navy indicates that a similar phenomenon occurs in a sector toward the sun at low sun angles during dawn and dusk (reference 6).

- The information content of IR images does not differ between black = hot and white = hot video polarity, nor between the false color options evaluated.

- The detection and classification distances obtained using the wide FOV option against the low profile targets in this field test was insufficient for CG applications. The 7-degree FOV available with the Agema sensor provided the narrowest of the wide FOVs evaluated.

- A narrow FOV will be required to obtain the detection and classification distances required for CG operations. Operation of the sensor array used in this field evaluation demonstrated the difficulty of locating objects with a two-degree FOV, even with *a priori* knowledge of their location. It would most likely be ineffective to manually search for targets more than a few nmi distant using a narrow FOV.

- This test series demonstrates that representative detection and classification distances can be calculated for low profile targets of CG interest when environmental conditions and sensor parameters are known (see also reference 5).

CHAPTER 5

5.0 RECOMMENDATIONS

The following recommendations are based on the results obtained from the preliminary phase of this testing:

- For applications of IR technology in warm humid climates, MWIR sensors provided the longest detection distances and are considered superior to LWIR sensors for these longer distance and higher humidities.

- The CG should conduct a similar field test in the Long Island Sound region during the late fall or early spring when air and water temperatures are lower and solar energy levels are lower and less direct. Theoretically, LWIR sensors outperform MWIR sensors in cooler climates. The CG should try to measure these performance differences prior to selecting a sensor system to employ fleet wide.

- Several IR systems are available that incorporate lens filters. The CG should select filters that enhance the sensors' abilities, especially in marginal situations. As an example, a lens filter that eliminates the problems associated with solar glint is available for MWIR sensors. The CG should investigate these filters to determine to what extent they alter other image data.

- The CG need not require false color modes for their operational requirements. The option of selecting between black = hot and white = hot video polarity is sufficient.

- The CG should investigate the use of computerized auto-acquire modes to notify operators of potential targets within a FOV. This capability would permit the use of larger lens combinations and would provide greater detection and classification distances without minimizing search coverage.

- Based on a maximum empirical IR detection distance of 10 nmi, the CG should investigate slaving the IR sensor to the ships' radar in order to point the system at radar targets as they enter the effective range of the sensor.
- The CG should investigate algorithms that can recognize geometric forms to enhance an operator's ability to classify target vessels.
- Due to the complexities of the IR scene, the CG should not rely entirely on theoretical performance factors for selecting an IR system for implementation onboard CG units. After eliminating those systems that are the least capable of those currently available, side-by-side evaluation of potential systems in the field should be performed.
- Utility of an IR system cannot be judged solely on the detection and classification distances achieved. Any evaluation of IR systems must include an assessment of the reliability and ease of operation.

REFERENCES

1. Plourde, J.V., Summary Report for the Installation and Field Evaluation of the Shipboard Infrared Imaging System (SIRIS), Analysis & Technology, Inc. for the CG Research and Development Center, (in review, Dec 1995).
2. Wolfe, W.L., ed. "The Infrared Handbook", Environmental Research Institute of Michigan and Office of Naval Research, 1983.
3. Kneizys, F.X., et.al., "Atmospheric Transmittance/Radiance Computer Code LOWTRAN 6", Optical Physics Division, AFGL 1983
4. Moser, P.M., "Mathematical Model of FLIR Performance", NAVAIRDEVCEN Technical Memo NADC-20203:PMM, ADA 045247, 1972
5. Skowronek, P., Paolino, R.N., and Plourde, J.V., Application of Infrared Sensing Technology to U.S. Coast Guard Counter Narcotic Mission, Proceedings of the 1995 ONDCP International Symposium Counter-Drug Law Enforcement, 1995.
6. Caulfield, J.T., Pauli, M.R., Michaels, S.P., Wilder, E.L., and York, R.A., Observation and Extraction of Faint Infrared Targets Near the Horizon, Proceedings IRIS Targets, Backgrounds and Discrimination, Vol II, 1994.

BLANK

APPENDIX A

OVERVIEW OF IR PHENOMENOLOGY

Infrared energy is electromagnetic energy much like visible light, but because of its longer wavelengths, it is invisible to the naked eye. Reference 1 provides an extensive review of IR phenomenology. A task-related overview directed towards this project is presented here.

Remote sensing of thermal energy at IR wavelengths is usually confined to spectral regions, called atmospheric windows, where the atmosphere is sufficiently transparent to allow radiation to travel over significant path lengths with little absorption or scattering. These atmospheric windows exist in the 3 to 5 micrometer (μ) wavelength band known as medium wave infrared (MWIR), and the 8 to 12 μ wavelength band known as long wave infrared (LWIR). Strong absorption bands, resulting principally from atmospheric water vapor and carbon dioxide, effectively prohibit thermal remote sensing outside these regions.

While reflected radiation (from the sun or other light sources) dominates the visible spectrum, naturally emitted radiation dominates the IR spectrum. IR energy radiated from an object is the sum of its self-radiated energy, thermal energy reflected off it, and thermal energy transmitted through it. Each of these three components is governed by the properties of the materials of any particular object. Target materials (e.g., wood, fiberglass and steel) and the water background are considered opaque at IR wavelengths and energy transmitted through each is negligible. At night, when the main source of reflected energy and differential heating (the sun) is removed, objects cool and much smaller thermal differences between dissimilar materials are typically experienced. For objects at the same temperature, the main source of thermal contrast are the relatively

small differences in emissivity (the ratio of the radiance of a given object to that of a perfect emitter). The value for emissivity is rated from 0 to 1. The greater the emissivity, the warmer the object will appear against a given thermal background. The greatest benefit from thermal imaging is experienced during a poorly lighted or nighttime scene.

Assuming a perfectly transparent atmospheric window, if the thermal difference (contrast) between an object and its background is greater than the sensitivity of a sensor, then the object will be detectable with the sensor until it is too small to illuminate a detector element. The physical size of an object is not the only factor that determines if an object can be displayed in the FOV provided. A very high contrast target may only subtend a portion of a detector element but may possess sufficient energy to illuminate the entire detector element (thermal blooming).

The atmosphere is not perfectly transparent, and the level of transmission varies with electromagnetic wavelength, atmospheric moisture, and atmospheric pollutants. Water greater than approximately 0.03 centimeters thick is opaque at IR wavelengths (reference 1). Atmospheric moisture in the form of rain and fog (actual water droplets) degrades atmospheric transmission to a greater extent than the gaseous forms of atmospheric moisture (i.e., haze). This atmospheric transmittance has been modeled and the model is known as LOWTRAN (reference 2). LOWTRAN-6 software was used for the calculations performed in this evaluation. The actual distance at which an object can be displayed by a particular sensor depends on a combination of several parameters, including: sensor sensitivity, actual thermal contrast, and atmospheric transmittance in the sensor's wave band.

An important and often misunderstood characteristic of an IR scene is that the source of an IR signature is not always evident and is easy to misinterpret. The IR sensor only detects the thermal signature of the surface being viewed and that thermal signature can be dominated by an object behind or adjacent to the actual surface being viewed. Two examples follow:

(1) Solar energy warming of a shallow sandy coastal area can create a thermal gradient between the near coastal waters and water a few hundred yards from shore. This gradient closely resembles the visible spectrum contrast between shallow and deeper water. Because water severely attenuates thermal energy propagation, the IR scene is not depicting bottom structure, but rather the effect of solar energy heating the bottom and shore structure. The interaction of shore structure and bottom heating with the near coastal water creates the thermal contrast.

(2) In a close-up of a vessel, an IR image of the holding tanks and engine spaces can often be detected on the hull as thermal differences, but the sensor is not detecting the engine or seeing into the tanks. It is merely detecting thermal contrast on the hull. *A priori* knowledge of vessels allows the observer to conclude that the contrast is due to engine heat or holding tank thermal characteristics (warm or cool).

Two measurements typically used to describe IR sensor sensitivity are minimum resolvable temperature difference (MRTD) and noise-equivalent temperature difference (NETD). The MRTD is a somewhat subjective measurement of an operator's ability to detect very small thermal differences with the sensor. The NETD is a more objective measure of the sensor system noise level and quantifies the minimal signal required above the noise to illuminate detector elements.

As noted above, there are two main atmospheric windows typically used for IR sensors. Sensors operating in either atmospheric window are subject to the conditions of their bandwidth. For example, at near-ambient temperatures (27°C), the energy radiated by a nonspecific body is greater at LWIR wavelengths than at MWIR wavelengths (see figure A-1). This power density function will shift for objects at different temperatures; however, for the near-ambient (27°C) target temperatures during this test the curve adequately estimates the target power density function. Figures A-2 and A-3 illustrate the effect of relative humidity on transmission of thermal energy at different wavelengths. Atmospheric transmission of LWIR energy is more significantly degraded than MWIR

transmission with increasing relative humidity. As relative humidity increases toward 100 percent, atmospheric transmission continues to decrease. Figures A-4 and A-5 depict the result when the atmospheric transmission curves in figures A-2 and A-3 are applied to the power density function presented in figure A-1. The power density curves depicted in figures A-4 and A-5 indicate that for a typical boat target at a distance of 12 km, more thermal energy reaches an MWIR sensor than reaches an LWIR sensor as relative humidity increases.

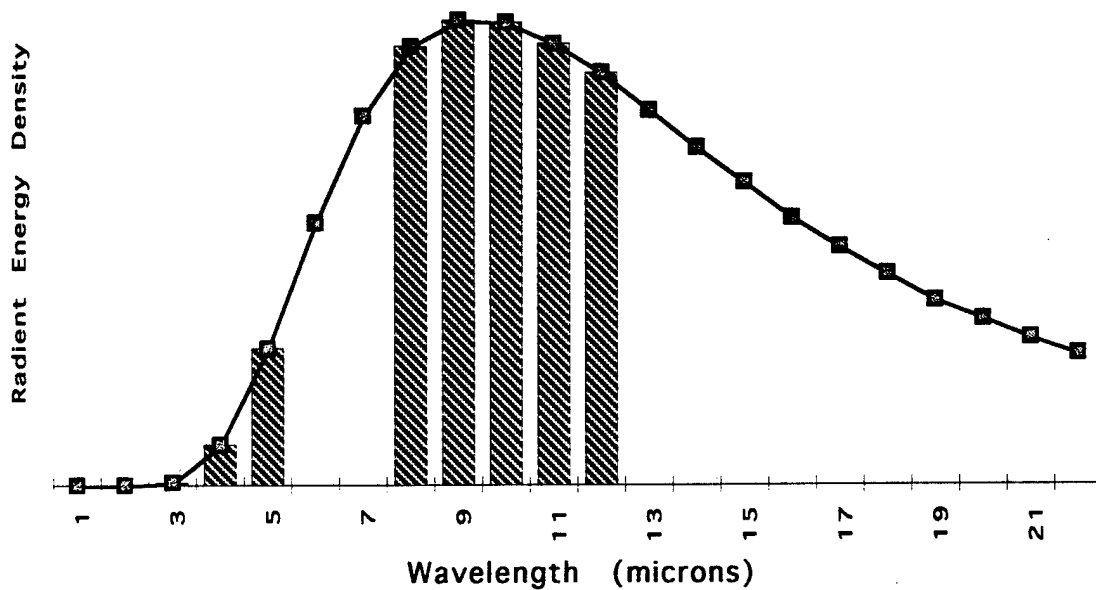


Figure A-1. Radiant Energy versus Wavelength (at 27°C)

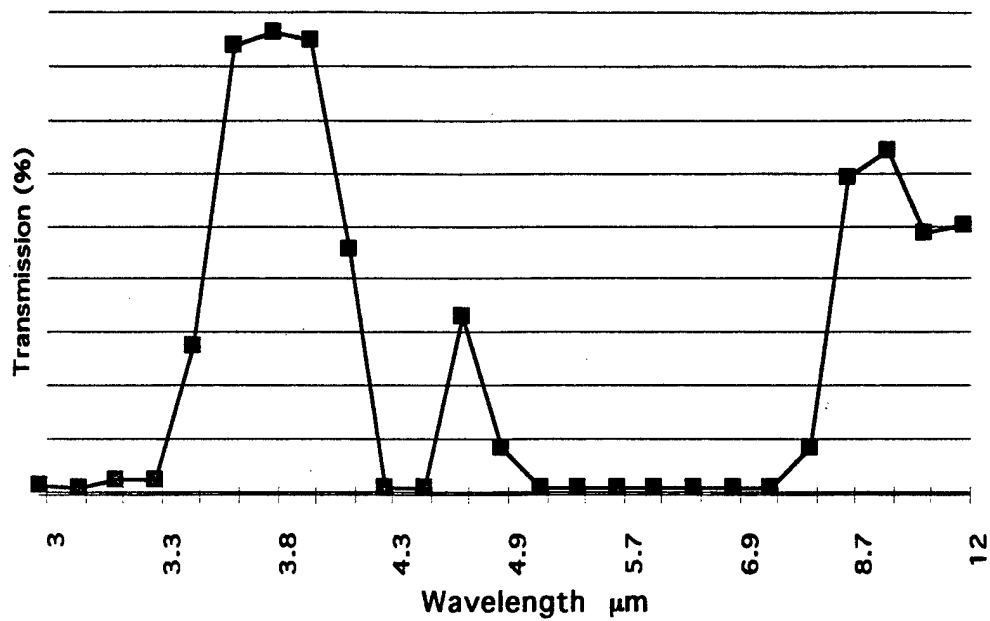


Figure A-2. Atmospheric Transmission versus Wavelength
(Range = 12 km, RH = 50%)

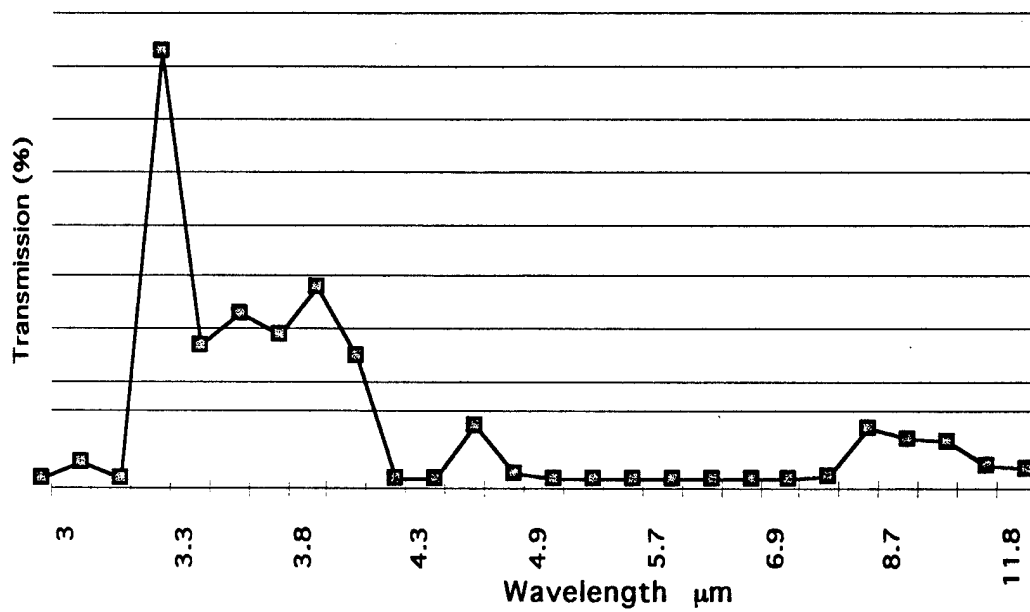


Figure A-3. Atmospheric Transmission versus Wavelength
(Range = 12 km, RH = 76%)

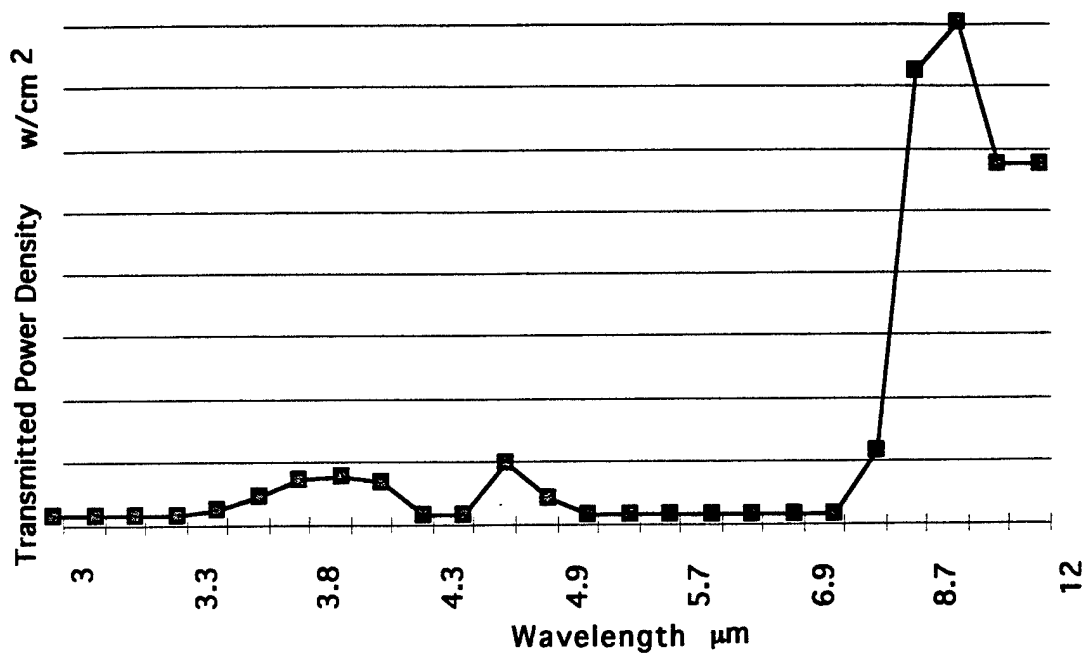


Figure A-4. Transmitted Power Density versus Wavelength
(Range = 12 km, RH = 50%)

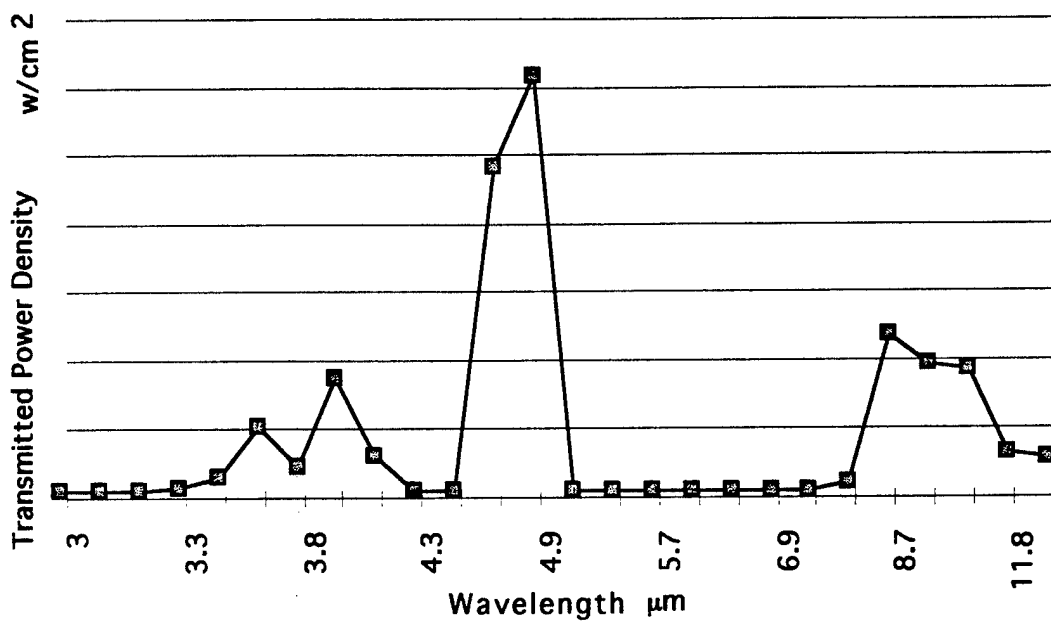


Figure A-5. Transmitted Power Density versus Wavelength
(Range = 12 km, RH = 76%)